SANDIA REPORT

SAND2005-0339
Unlimited Release
Printed February 2005

Uncertainty Analysis of Heat Flux Measurements Estimated Using a One-Dimensional Inverse Heat Conduction Program

Victor A. Figueroa, James T. Nakos, and Jill E. Murphy

Prepared by
Sandia National Laboratories
Albuquerque, New Mexico 87185 and Livermore, California 94550

Sandia is a multiprogram laboratory operated by Sandia Corporation,
a Lockheed Martin Company, for the United States Department of Energy's
National Nuclear Security Administration under Contract DE-AC04-94AL85000.

Approved for public release; further dissemination unlimited.

Sandia National Laboratories

Issued by Sandia National Laboratories, operated for the United States Department of Energy by Sandia Corporation.

NOTICE: This report was prepared as an account of work sponsored by an agency of the United States Government. Neither the United States Government, nor any agency thereof, nor any of their employees, nor any of their contractors, subcontractors, or their employees, make any warranty, express or implied, or assume any legal liability or responsibility for the accuracy, completeness, or usefulness of any information, apparatus, product, or process disclosed, or represent that its use would not infringe privately owned rights. Reference herein to any specific commercial product, process, or service by trade name, trademark, manufacturer, or otherwise, does not necessarily constitute or imply its endorsement, recommendation, or favoring by the United States Government, any agency thereof, or any of their contractors or subcontractors. The views and opinions expressed herein do not necessarily state or reflect those of the United States Government, any agency thereof, or any of their contractors.

Printed in the United States of America. This report has been reproduced directly from the best available copy.

Available to DOE and DOE contractors from
U.S. Department of Energy
Office of Scientific and Technical Information
P.O. Box 62
Oak Ridge, TN 37831

Telephone: (865)576-8401
Facsimile: (865)576-5728
E-Mail: reports@adonis.osti.gov
Online ordering: http://www.osti.gov/bridge

Available to the public from
U.S. Department of Commerce
National Technical Information Service
5285 Port Royal Rd
Springfield, VA 22161

Telephone: (800)553-6847
Facsimile: (703)605-6900
E-Mail: orders@ntis.fedworld.gov
Online order: http://www.ntis.gov/help/ordermethods.asp?loc=7-4-0#online

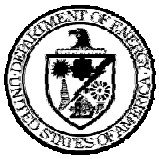

SAND2005-0339
Unlimited Release
Printed February 2005

Uncertainty Analysis of Heat Flux Measurements Estimated Using a One-Dimensional, Inverse Heat-Conduction Program

V.G. Figueroa and J.T. Nakos
Fire Science and Technology, Department 9132
Sandia National Laboratories

J.E. Murphy
Worcester Polytechnic Institute

Abstract

The measurement of heat flux in hydrocarbon fuel fires (e.g., diesel or JP-8) is difficult due to high temperatures and the sooty environment. Un-cooled commercially available heat flux gages do not survive in long duration fires, and cooled gages often become covered with soot, thus changing the gage calibration. An alternate method that is rugged and relatively inexpensive is based on inverse heat conduction methods. Inverse heat-conduction methods estimate absorbed heat flux at specific material interfaces using temperature/time histories, boundary conditions, material properties, and usually an assumption of one-dimensional (1-D) heat flow. This method is commonly used at Sandia's fire test facilities. In this report, an uncertainty analysis was performed for a specific example to quantify the effect of input parameter variations on the estimated heat flux when using the inverse heat conduction method. The approach used was to compare results from a number of cases using modified inputs to a base-case. The response of a 304 stainless-steel cylinder [about 30.5 cm (12-in.) in diameter and 0.32-cm-thick (1/8-in.)] filled with 2.5-cm-thick (1-in.) ceramic fiber insulation was examined. Input parameters of an inverse heat conduction program varied were steel-wall thickness, thermal conductivity, and volumetric heat capacity; insulation thickness, thermal conductivity, and volumetric heat capacity, temperature uncertainty, boundary conditions, temperature sampling period; and numerical inputs. One-dimensional heat transfer was assumed in all cases. Results of the analysis show that, at the maximum heat flux, the most important parameters were temperature uncertainty, steel thickness and steel volumetric heat capacity. The use of a constant thermal properties rather than temperature dependent values also made a significant difference in the resultant heat flux; therefore, temperature-dependent values should be used. As an example, several parameters were varied to estimate the uncertainty in heat flux. The result was 15-19% uncertainty to 95% confidence at the highest flux, neglecting multidimensional effects.

Acknowledgements

This project was supported by the Weapons Systems Engineering Certification Program (known as Campaign 6) and Readiness in Technical Base and Facilities (RTBF) Programs. The authors gratefully acknowledge this support. Technical input from James Beck, Beck Engineering Consultants, Okemos, MI (retired professor, Michigan State University), the author of the inverse-heat-conduction program, and from Walter Gill, Fire Science & Technology Dept 09132, was very helpful. In addition, technical reviews by Ben Blackwell, SNL Org. 09133, Validation & Uncertainty Quantification (retired February 2004) and Ned Keltner, Ktech Corp., are gratefully acknowledged.

Table of Contents

List of Figures

List of Tables

Nomenclature

1-D	One-dimensional
2-D	Two-dimensional
3-D	Three-dimensional
DAS	Data acquisition system
GUI	Graphical user interface
IHCP1D	Inverse Heat Conduction Program 1-Dimensional
JP-8	Jet fuel
PC	Personal computer (IBM compatible)
RSS	Root-sum-square
SNL	Sandia National Laboratories
SODDIT	Sandia One Dimensional Direct and Inverse Thermal program
SS	stainless steel
TCs	thermocouples
UMF	Uncertainty magnification factor

I. Introduction

A. Purpose

This report presents the results of an uncertainty analysis associated with use of an inverse heat conduction program to determine the heat flux for a single geometry and fire condition. The code used was called "Inverse Heat Conduction Program 1-Dimensional (IHCP1D)," Version 7.0 [1]. Other inverse heat-conduction programs are available, e.g., Sandia One Dimensional Direct and Inverse Thermal program (SODDIT) [2], but IHCP1D was chosen because it is commercially available, has a graphical user interface (GUI), and can be used on an IBM-compatible personal computer. It is important to determine how uncertainties in temperature measurements, material geometries, material properties, or code-input parameters can affect the estimation of heat flux when using an inverse heat conduction code.

If the estimated uncertainty of the heat flux is well characterized for this frequently employed calorimeter design, then it also is possible to use the results to predict heat flux measurement uncertainties in future tests held under similar conditions. This analysis also will help define which (of the many) parameter inputs are most critical to the total uncertainty and therefore help focus efforts to reduce the uncertainty.

B. Literature Review

In general, the inverse method is very sensitive to both temperature measurement and thermal-property variations. Mathematically, inverse methods are "ill-posed," i.e., their solution does not satisfy requirements of existence, uniqueness, and stability under small changes in input parameters [3]. Hence, it was important to understand effects of the changes in input parameters on inverse heat flux calculations.

In [4], errors were evaluated when 1-D inverse heat flux techniques were applied to problems involving 2-D heat-transfer for a 150 cm (60 inch) diameter cylindrical calorimeter in a fire. The degree of localized heat flux was controlled using a circumferential heat flux boundary condition. Results were compared against a 2-D finite-difference model. This study found that errors in inverse heat flux calculations ranged between 0.5% and 18%, depending on how localized (i.e., spatially concentrated) the heat flux was on the outer surface of the calorimeter. Therefore, 2-dimensional effects can be large.

The effects of temperature measurement random errors (from noise in the data acquisition system digital voltmeter) on inverse heat flux calculations were analyzed in [5] for a flat plate configuration. An analytical solution for a triangular pulse was studied. In [5], when controlled random noise was introduced to the temperature history input, error magnitudes in the inverse heat conduction solution increased linearly with the noise level of the input signal. After noise was added into the temperature input history, a cubic spline was used to smooth the noisy input data. This smoothing step was effective in reducing the heat flux error when the noise was larger than about 1/3 of the maximum data acquisition system random error (assumed to be ±2°F in

[5]). When the random noise was smaller, this smoothing step increased the solution error slightly above errors seen prior to the smoothing. For a ±2°F noise level, the heat flux error was as high as 29% for a low thermal diffusivity material, and as low as 11% for a high diffusivity material. For small noise levels (i.e., ±0.1°F), the errors were 2% for a low diffusivity material, and 1% for a high diffusivity material.

Uncertainty in inverse heat flux calculations for a 30 cm diameter cylindrical configuration in a fire resulting from uncertain construction, uncertain temperature dependent thermal properties, numeric input parameters and temperature measurement uncertainties were not analyzed in the references cited.

II. Experimental Configuration and Data

The measurement device used as the basis for this analysis was a 30.5-cm-diameter (12-inch) × 40.6-cm-long (16-inch) cylindrical tube called a "calorimeter." The calorimeter was made from 0.32-cm-thick (1/8-in.) 304 stainless steel (SS). The inside was filled with multiple layers of 2.5-cm-thick (1-in.) "Kaowool" insulation (made by Thermal Ceramics, Inc.). Figure 1 shows a sketch of the calorimeter. Thermocouples (TCs) were mounted inside the calorimeter at locations shown in Figure 1.

All TCs were Type K (chromel-alumel), 1/16-in. diameter, Alloy 600 sheath, with MgO insulation. Intrinsic thermocouples (TCs) were used to measure temperature on the unheated side (i.e., inside) at the SS-insulation interface. Intrinsic TCs were made by stripping the Alloy 600 sheath away and exposing the individual wires. Each wire (chromel and alumel) was then individually spot welded to the SS surface being measured. This type of TC installation was believed to be the most accurate for this application. Ungrounded, mineral-insulated, metal-sheathed TCs were also placed 1 inch from the SS wall, in the insulation, see Figure 1. All TC leads were routed parallel to isotherms towards an end plate, and then routed through a slot in the plate.

During the experiment, the outer SS surface (x = L) was subjected to the heat flux (q) from the fire, see Figure 2. Heat was conducted into the calorimeter. The steel temperature measurement was performed at the interface between the steel and insulation. Another temperature measurement was made in the insulation, 1 inch from the steel interface (so-called "insulation-insulation" interface, at x=0). The remainder of the inside of the calorimeter was filled with a roll of 1-in. thick insulation. As stated earlier, 1-D conduction was assumed in this analysis. Two- (2-D) or three-dimensional (3-D) effects were assumed negligible, but may not be in all applications, e.g., when the heat flux vary strongly along the perimeter of the calorimeter. Two-dimensional effects were discussed in reference [4].

The fire experiment was conducted using a 3.1 × 4.3 m (10 × 14 ft) rectangular pan about 7 m (23 ft) from the calorimeter. The pan was filled with gravel up to 1-inch below the top lip. JP-8 fuel was poured into the pan until the top surface was ¼-inch above the top of the gravel (see Figure 3).

The pan and the calorimeter were inside a 7.3 × 16.5 m (24 × 54 ft) rectangular fire test enclosure (FTE). The pan was located near the FTE doors, while the calorimeter was located about 7 m away, farther into the FTE. Entrained air flowed over the pan fire towards the calorimeter, but the flame zone never reached the calorimeter. However, very hot combustion gases (e.g., 1,000°C or higher) were present over the FTE's upper layer [4.5 m (14.6 ft) high], resulting in a heat flux to the calorimeter's upper surface. Only data from the upper surface of the calorimeter was used in this study.

Calorimeter #1 was used in this analysis. It was located in the upper left corner of a FTE (see Figure 3). The calorimeter was mounted with the cylindrical axis horizontal. The axis was located about 1 m (3 ft) above the floor.

Temperature data were measured at 1 second intervals. Temperature data from these thermocouples are shown in Figure 4. After a vigorous initial burn (see temperature spike in Figure 4), the fire intensity decreased because the fuel level dropped below the top of the gravel bed. The calorimeter temperature then dropped sharply from about 670°C to 500°C. A slow, steady decline in temperature followed the sharp decrease in temperature. The slow decline in temperature was due to slow fuel burn rate through the fuel-gravel section of the pan.

The leader data were analyzed to determine the initial noise levels for the data acquisition system. For 150 sec before the fire started (between about 800-950 sec on Figure 4), the average temperature of the SS-insulation TC was about 19.42°C with a standard deviation of only 0.071°C. So, for 95% confidence the noise was about 0.14°C. Because this level is small, it will be assumed that the error from this source is accounted for by using a bias error of 5% (see Section IV.A.2).

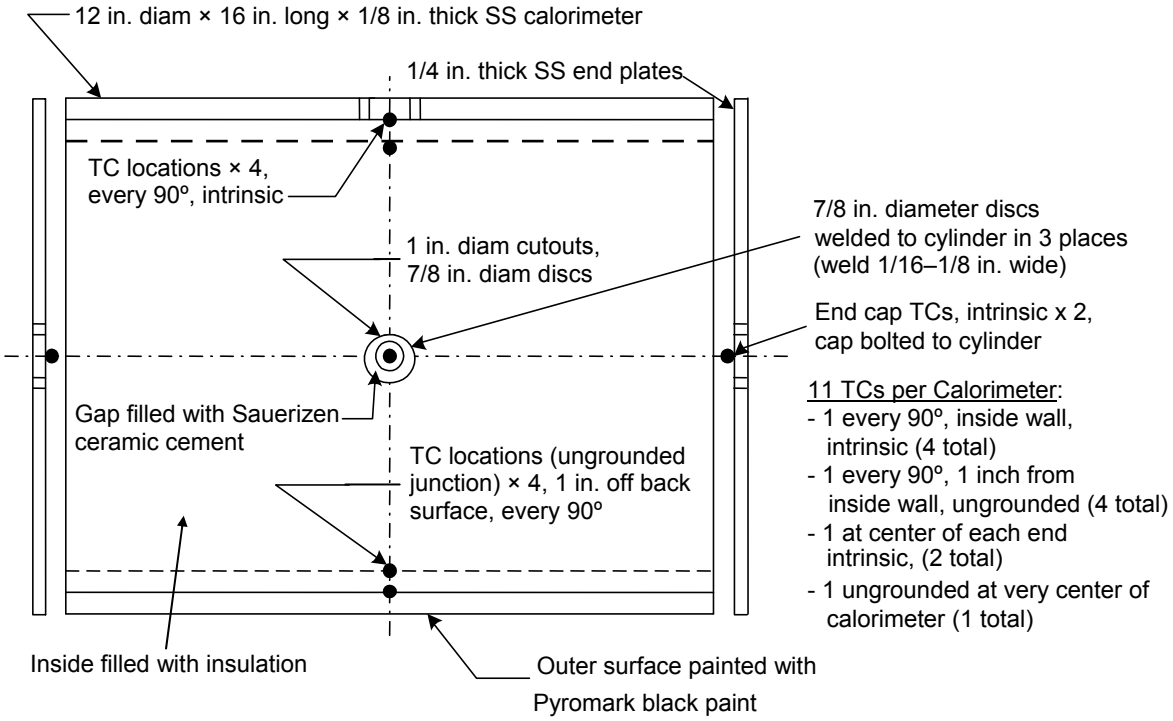

Figure 1: Side view of cylindrical calorimeter.

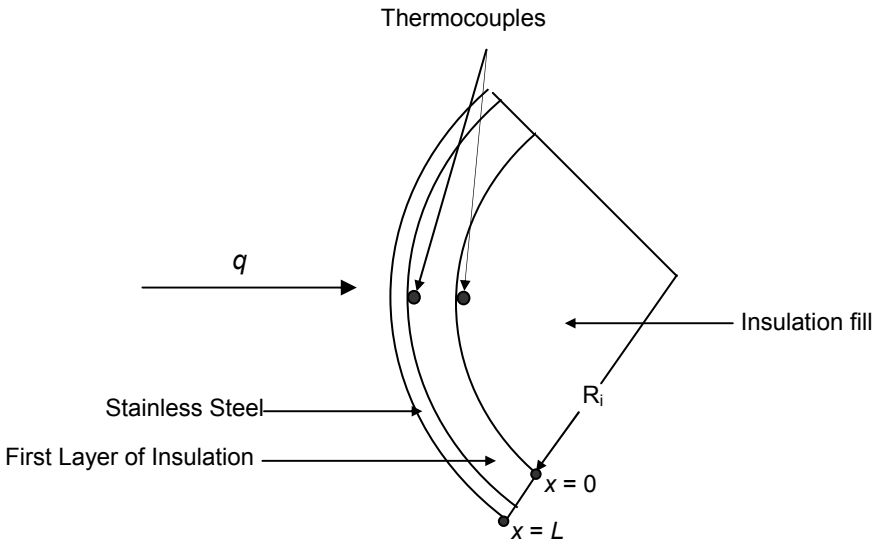

Figure 2: Calorimeter Sectional View.

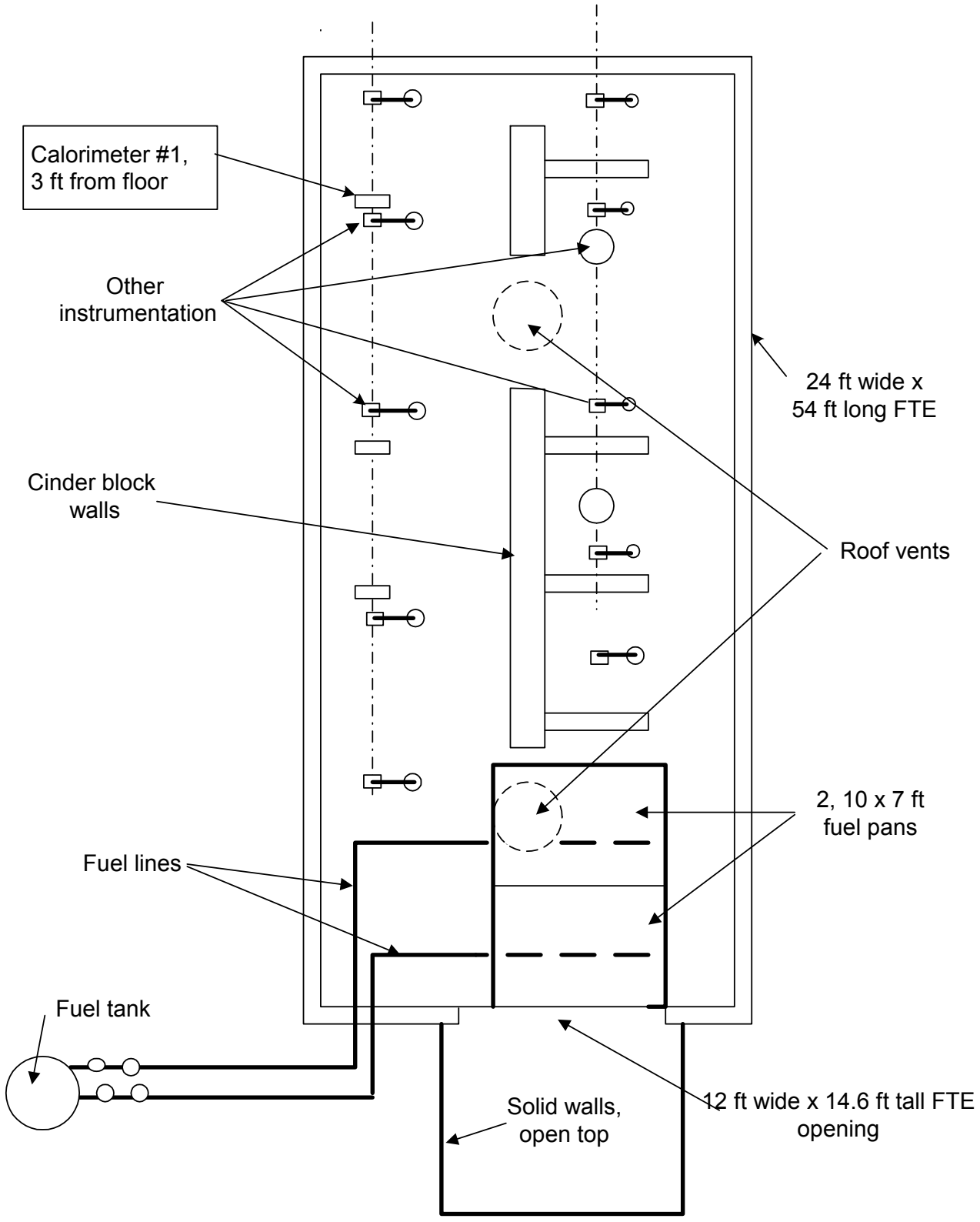

Figure 3: Fire Test Enclosure Layout.

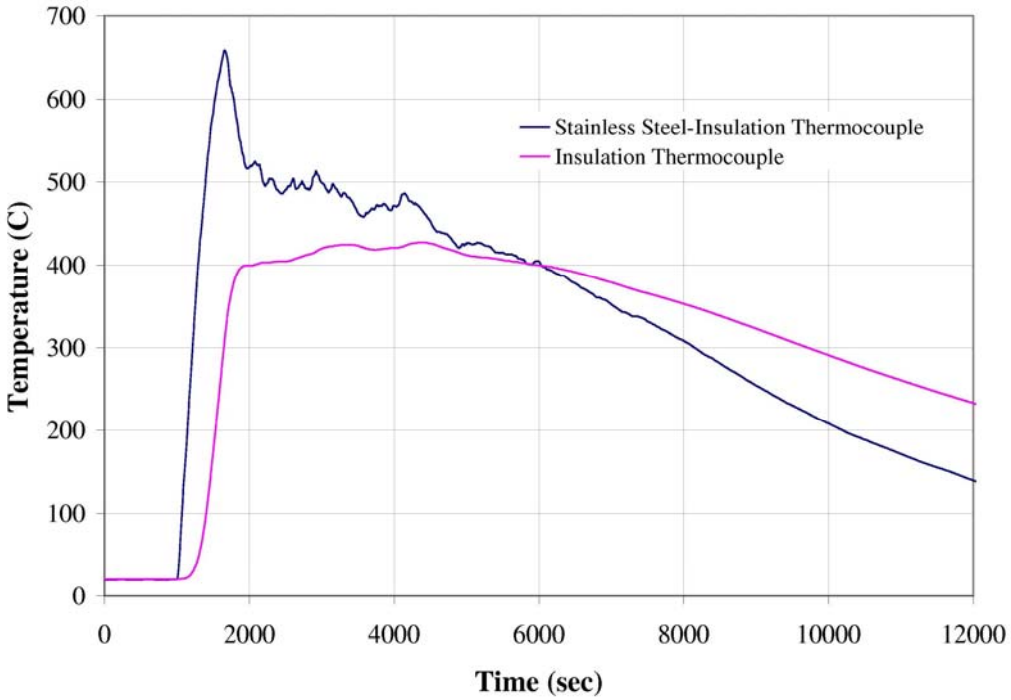

Figure 4: Temperature data from cylindrical calorimeter.

III. Methodology

In this study, the uncertainty in absorbed heat flux resulting from uncertain input parameters for a typical cylindrical calorimeter exposed to a fire was quantified. Incident heat flux on a surface is usually the parameter of interest, but the inverse heat conduction method estimates the absorbed flux. The conversion to incident flux requires an energy balance and estimation of other parameters (e.g., surface temperature, emissivity, and convection heat transfer coefficients). Estimation of the uncertainty of incident heat flux, given absorbed flux, is beyond the scope of this report and will be addressed in future work.

A first-order numerical perturbation method was used to perform the uncertainty analysis [6, 7]. In this method, only one parameter was changed per run. A scenario was chosen as a "base-case" and comparisons were made to the base-case to determine which input parameters had the largest effect on the estimated heat flux. The value for each input parameter was varied based on engineering judgment and measured variability (when possible). Only one parameter value was changed for each case, allowing for an unambiguous comparison. A typical run took only 5-10 seconds on a PC, which allowed for many runs in a short period of time. It was assumed that the results were uncorrelated—the estimated heat flux when varying one parameter was unaffected by other parameters. This assumption might not have been strictly true (e.g., variations in temperature measurements causes variation in thermal properties), but was used for expediency.

The IHCP1D program is a 1-D, inverse heat conduction program that calculates the absorbed (or "net") heat flux at a specified location given transient temperature histories. The surface heat flux is estimated using a 1-D formulation. Pertinent input parameters include:

- Material geometry (e.g., thickness),
- Material thermal properties (e.g., thermal conductivity, specific heat),
- Temperature measurements,
- Numeric parameters (e.g., number of future times, number of nodes, etc.), and
- Boundary conditions.

For this analysis, each input parameter was varied independently of the other parameters to determine the effect on the estimated heat flux. All varied cases were compared to a "base-case." Inputs for the base-case were chosen to provide results expected to be the most accurate. Selection of these inputs required some level of engineering judgment.

Absorbed heat flux was the parameter of interest. Two or 3-dimensional, and nonlinear effects were not considered. For small changes in input parameters, nonlinear effects are most likely negligible. Some parameters were changed by a large amount (e.g., insulation thermal conductivity), but nonlinear effects were still neglected.

Table 1 shows code-input parameters chosen for the base scenario run. The left column gives the required (step-by-step) input, while the right column lists the value used for that parameter in the analysis. Entries in Table 1 can be compared with each of the GUI inputs shown in Appendix A.

Geometric parameters and units are defined in Step 1. Region material numbers are No. 1 and No. 2 for the insulation and stainless steel, respectively. This program allows a maximum of 16 regions. As previously stated, the region thicknesses were 1 in. (0.0254 m) for the insulation and 1/8 in. (0.003175 m) for the steel. As previously stated, the calorimeter center was filled with insulation. However, the extra layers of insulation made a negligible difference in the results, so they were not included in the model. The number of nodes per region was arbitrary; however, the maximum number possible for all regions combined is 101 nodes. Thirty nodes per region were selected for the base-case.

Step 2 required the user inputs for the time step, time intervals, length of time, and number of future times. The IHCP1D manual [1] does not give adequate insight on how to select an appropriate value for the "calculated time steps per measurement time step". The default value of 10 was chosen for the base-case. Additional runs were performed to examine the effect of this parameter on the heat flux calculations. Results show the heat flux is not sensitive to this parameter.

For most inverse heat-conduction problems, including this one, the "number of time intervals with various future time steps" is set to one. When the number of time intervals is greater than one, the time domain is divided into the specified number of subintervals. For each subinterval, the user inputs numeric parameters (i.e., number of future times-see below) appropriate for the subinterval. This option allows the user to adjust the numeric parameters with the time varying

thermal characteristics of the problem. One interval was used for these calculations. The time at the end of the test was 12,600 seconds (3.5 hours).

Table 1: Base-Case Input Values

Steps	Base Scenario	Steps	Base Scenario
Step 1		**Step 4**	
Main geometry	Cylindrical radial	No. of columns of data	1
Units	W-kg-m-sec-C	**Step 5**	
No. of regions	2	**Material No. 1 (SS)**	
Region Material No.	1, 2	No. of components of *k** table	11
Region thickness (m)	0.0254; 0.003175	No. of components of ρC_p** table	11
No. of nodes/region	30, 30	Temperatures	0-1000°C in 100°C increments
Step 2		*k*(T)	0.0174T+14.11
Calculated time steps/measured time steps	10	ρ (T) x C_p(T)	$2.20e\text{-}3T^3 4.03T^2 + 3305.26T + 3676199$
No. of time intervals with various future time steps	1	**Material No. 2 (Kaowool)**	
		No. of components of *k** table	11
Time at end of interval	12,600	No. of components of ρC_p** table	11
		Temperatures	0-1000°C in 100°C increments
No. of future time steps	3	k(T) ρ (T) x C_p(T)	$9.43E\text{-}11T^3 + 4.67E\text{-}08T^2 + 1.14E\text{-}04T + 2.84E\text{-}02$ $100978 + 50.66T - 0.0146T^2$
Step 3			
Unknown boundary location	$x = L$		
Known boundary type	Prescribed temp.	**Step 6**	
		Calc. unknown *h*	NA
		Fin effect	Insulated sides

*k = thermal conductivity
**ρC_p = thermal capacity

The last input parameter in Step 2 was the number of future time steps. The IHCP1D program manual suggests use of the following equation as a first estimate of the number of future time steps:

$$r = 1 + 0.18\frac{1}{Fo}, \qquad (1)$$

where *r* is the number of future time steps, and *Fo* is the Fourier number. '*r*' is always an integer number. The Fourier number is given by:

$$Fo = \frac{\alpha \Delta t}{E^2}, \tag{2}$$

where α is the thermal diffusivity, Δt is the data sample rate, and E is the sensor depth below the heated surface. When the number of future times is small, calculations using the IHCP1D program become more unstable. Assuming the smallest possible value of Δt (1 second), and a ambient temperature value for α, $r = 2$. This is the minimum recommended number of future time steps required for stable calculations. The number of future time steps also depends on the standard deviation of temperature measurement variations. The greater the variations, the greater the future time step value. To add more stability, a value of 3 was used.

Boundary conditions were entered in Step 3. The first entry was the unknown boundary location. Only three choices were given: $x = 0$, $x = L$, and both $x = 0$ and $x = L$. The unknown boundary condition occurred at $x = L$, which was the surface exposed to the fire. The other boundary ($x = 0$) had a prescribed temperature history provided by the TC. Appendix B shows the input temperature data beginning at 800 seconds, about when the fire started.

The only item in Step 4 was the number of columns of data in addition to the time and SS-insulation temperatures. The data at $x = 0$, the insulation-insulation interface, provided an additional time varying, prescribed temperature-boundary condition, so the number of additional columns of data was set to 1.

Temperature dependent, material properties were entered in Step 5. Thermal conductivity and volumetric heat capacity values for each material were entered separately. It was possible to input up to 16 temperature values, with each temperature having a corresponding thermal property value. Eleven (11) values were used from 0°C–1,000°C in 100°C increments. The number of thermal conductivity values did not have to be equal to the number of volumetric heat-capacity values. For the base-case, temperature dependent values of both properties were used for both materials.[1] Table 1 shows temperature-dependent property equations. All equations were either 1st, 2nd, or 3rd order polynomials. Several additional cases used data with constant properties. Units for thermal conductivity were W/m-°C, for $\rho(T)$ were kg/m^3, and for $C_p(T)$ were J/kg-°C. Therefore, volumetric heat capacity had units of J/m^3-°C.

Step 6 of the program includes advanced features. Because no advanced features were used in this analysis, this feature was not used.

The last input step of the program is not shown in Table 1. It required the user to provide names for the input and output files, and to provide a header name for easy recognition of the output file. The input file contained prescribed temperatures from the experiment in text format.

[1] Properties for stainless steel were obtained from a private communication with Walter Gill, Sandia National Laboratories Department 09132. SS properties are consistent with previously published values. Properties for the insulation were obtained from Ned Keltner, Ktech Corp., and Roger Oxford, Thermal Ceramics, both in 2003. Insulation properties are believed to be the most complete of any data that are available.

Once this information was entered, the simulation was ready to run. As stated previously, a case typically took less than 10 seconds to complete on a PC. Results were displayed in the computer screen and also saved to memory. Results included the temperature and heat flux as a function of time at x = L, as well as other locations.

After results from the base scenario were calculated, the next step was to individually vary each parameter and recalculate the flux. Table 2 shows changes made for each case. The changed parameter was the only value that differed from the base-case; all other parameters were held constant.

Table 2: Input Changes from Base-case

Case	Changed Parameter	Change	Case	Changed Parameter	Change
Base	None	None	Base	None	None
2	No. of nodes/material	5	22	Insulation *k**	-25.0%
3	No. of nodes/material	10	23	SS ρC_p**	-2.5%
4	No. of nodes/material	30	24	SS ρC_p**	-5.0%
5	No. of calc./meas. time steps	5	25	SS ρC_p**	5.0%
6	No. of calc./meas. time steps	15	26	Insulation ρC_p**	5.0%
7	No. of calc./meas time steps	20	27	Insulation ρC_p**	25.0%
8	No. of future time steps	5	28	Insulation ρC_p**	-25.0%
9	No. of future time steps	10	29	SS *k**	Constant
10	No. of future time steps	20	30	SS ρC_p**	Constant
11	Stainless steel (SS) thickness	5.0%	31	SS *k** and ρC_p**	Constant
12	SS thickness	10.0%	32	Insulation *k**	Constant
13	SS thickness	-10.0%	33	Insulation ρC_p**	Constant
14	Insulation thickness	5.0%	34	Insulation *k** and ρC_p**	Constant
15	Insulation thickness	10.0%	35	SS /insulation temp.	-2.5%
16	Insulation thickness	-10.0%	36	SS /insulation temp.	2.5%
17	SS *k**	-2.5%	37	SS /insulation temp.	5.0%
18	SS *k**	2.5%	38	SS/insulation temp.	5°C
19	SS *k**	5.0%	39	SS /insulation temp.	+10°C
20	Insulation *k**	5.0%	40	SS /insulation temp.	-10°C
21	Insulation *k**	25.0%	41	Boundary conditions (see Appendix C)	Adiabatic

**k* = Thermal conductivity

***ρC_p* = Thermal capacity

IV. Results

A. Base-Case

1) General

The first run was the base-case scenario. Figure 5 shows the absorbed heat flux at the surface exposed to the fire ($x = L$). The maximum absorbed heat flux was about 20 kW/m^2 during the initial high intensity period. The absorbed heat flux became negative between 1,800 and 2,000 seconds because the fire was over and the calorimeter was radiating to the environment.

Other temperature measurements from the experiment (not shown) indicate the presence of a heat flux gradient around the calorimeter's circumference. These effects were neglected in this 1-D analysis. Since this was a comparative analysis, errors in the predicted heat flux caused by the 1-D assumption were assumed to have a negligible impact on the comparisons.

Another source of error is the difference between the measured and calculated temperatures at the SS-insulation interface. A good indicator of this error is the residual output of IHCP1D, which shows the difference between the calculated and actual temperature histories at the SS-insulation interface. Figure 6 shows residuals for the base-case. Maximum temperature differences occurred during the maximum heat flux period and were less than 6 degrees (less than 1% of the maximum temperature).

Since the absorbed heat flux was largest during the period between 800 and 2,000 seconds, the uncertainty analysis was most important in this time frame; therefore, the analysis focused in this period.

2) Base-case Error

This is a comparative analysis; that is, results of calculations with varied parameters were compared with the base-case. There is no reason to expect that in a problem such as this, IHCP1D (or any other inverse code) will predict the absorbed heat flux with no error. As shown in reference [1], comparisons of IHCP1D results with an exact solution for a triangular heat flux pulse had small errors during the rise and fall for 2, 3, and 4 future times, but were not exact at the peak. The error in peak heat flux was about 5% (from the figure in reference [1]), while the error during the rise and fall was negligible except for large future times. The heat flux in fires is often erratic, so may be approximated by a series of triangular pulses similar to the one in reference [1]. Therefore, for this case, it will be assumed that the base-case under predicts the maximum absorbed heat flux by 5%.

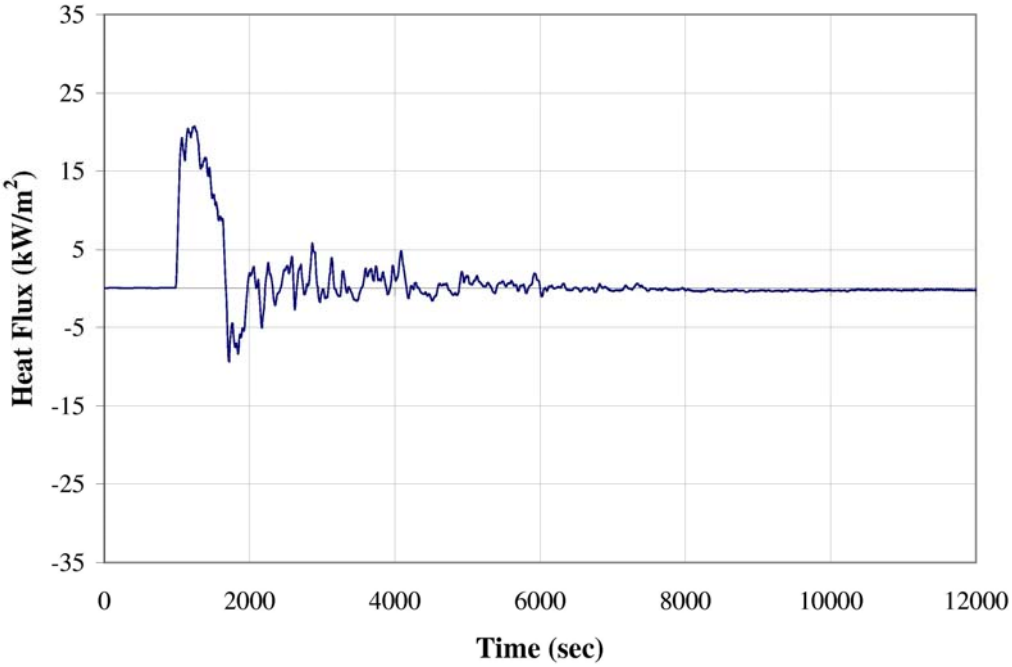

Figure 5: Heat flux at $x = L$ for base-case scenario.

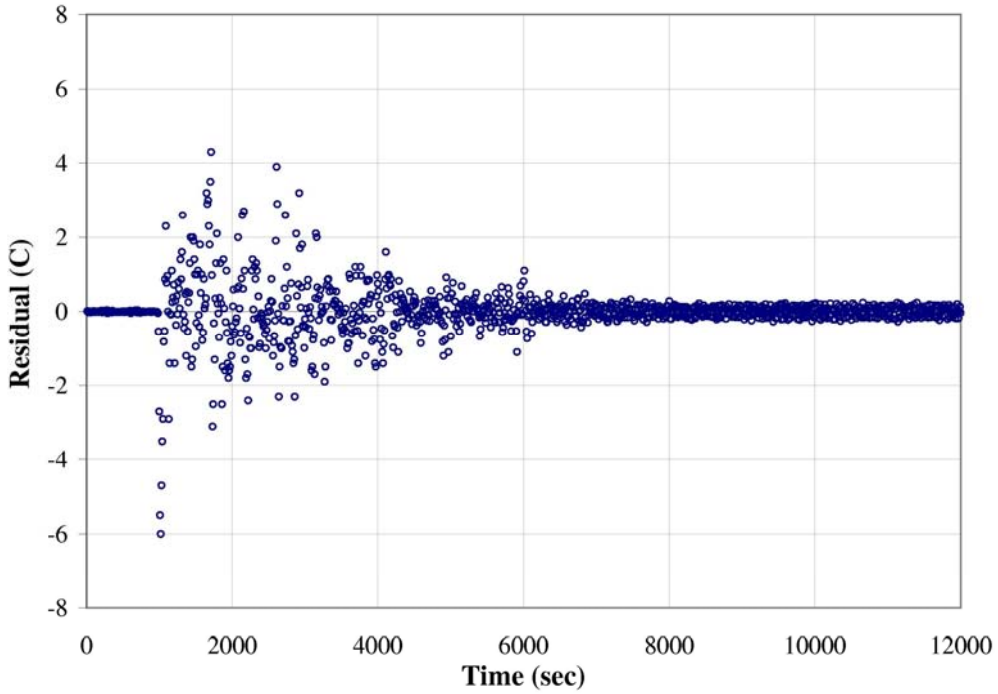

Figure 6: Residuals for the SS-insulation interface temperature estimates.

3) Effects of Data Sampling period on the Base-case Results

During the experiment, temperatures were recorded once every second using the data acquisition system (DAS) (sample rate = 1 sample/second). This sample rate was believed to capture sufficient amount of information (i.e., high frequency content). To study the effects of data sample rate on absorbed flux, the sample rate was changed from 1-second-per-sample to 5-, 10-, 20-, and 40-seconds-per-sample by decimating (eliminating data) the temperature histories. The heat flux was calculated for each of these sample rates.

Figure 7 shows absorbed heat flux for the period when the heat flux was highest (800 – 2,000 seconds). Each plot represents a different sample rate. The 1-second-per-sample data shows higher peaks and more fluctuations than either the 5 or 10 sec-per-sample data. The 1-second-per-sample data peaks may be real, or may be artifacts of small temperature variations. Because this calorimeter was about 7 m from the fire, it will be assumed that the 1-sec data fluctuations are due to noise amplification. Therefore, a longer sample period was used for the base-case (10-seconds/sample). When the sample period was increased from 1-sec-per-sample to larger values, the high-frequency fluctuations were smoothed out. Sample periods of 20 and 40 seconds resulted in a time shift of the heat flux curves at the beginning of the rise, which is undesirable, so neither of these rates were used. The time shift between the 5- and 10-second data was relatively small, with the 5-second data being the less damped. For this study, the data set with 10-seconds-per-sample was used.

The 1-second data, which showed large fluctuations, should be considered if the fluctuations are real flux variations. This might be the case if a calorimeter was directly in a fire. However, it is difficult to know if the fluctuations are "real" because the time constant of both the calorimeter and thermocouple have to be considered. A more thermally massive calorimeter will respond more slowly, and therefore higher-frequency fluctuations may not be captured. This is a draw-back of the inverse method: it is difficult to determine whether or not heat flux variations are real, or are artifacts of temperature fluctuations, the time constant of the calorimeter, or errors in the temperature measurements.

4) Sensitivity to Boundary Conditions (Step 3)

Temperature history obtained from thermocouples located in the 1" thick insulation layer 1 inch from the steel wall were used as boundary conditions (x = 0, see Figure 2) for the base-case. It is probable that the error of this temperature measurement is affected by the method of thermocouple installation. However, this additional error was neglected.

Two adiabatic boundary condition locations were examined to assess differences in the calculated heat flux at the exposed surface (x = L). Appendix C compares heat flux using adiabatic boundary conditions at two locations (x=0 and R_i=0) when compared with results from the prescribed temperature boundary condition. In the base-case, a temperature boundary condition was specified at x = 0 (Figure 2). One adiabatic boundary condition was assumed at R_i = 0 and the other at x = 0 (Figure 2). Results using both of these adiabatic boundary conditions were compared with the prescribed temperature results and show up to a 6% difference in heat flux when an adiabatic boundary condition is compared with results from the prescribed

temperature boundary condition. However, the 6% difference occurred only after the absorbed flux went negative (see Appendix C), when the fire was over. This result is not as important as the flux when the fire was ongoing. The error when the fire was ongoing (time < 2000 sec) was less than 0.2%, which is negligible. This result suggests that either adiabatic boundary condition is acceptable if one is only interested in the surface heat flux (at x = L) during the fire. Therefore, the extra TC at the insulation-insulation interface may be eliminated if cost or lack of space is a consideration. However, it is recommended that this TC be used because information from this TC provides a better characterization of the boundary condition, and can provide insight on 2-dimensional conduction in the insulation layer. However, installing TCs in the insulation at x=0 (see Figure 2) should be done with care. For low conductivity materials, temperature disturbances due to the TC may be very large, and therefore the TC reading can have a large error [8]. Therefore, TCs in low conductivity materials should be mounted with care.

During the experiment, the heat flux to the surface varied considerably around the circumference, so there was no reason to believe there would be an adiabatic-boundary condition at either $R_i = 0$ or x = 0. Also, no insulation is perfectly adiabatic. Therefore, for the analysis, the prescribed temperature-history boundary condition at $x = 0$ was used for all cases.

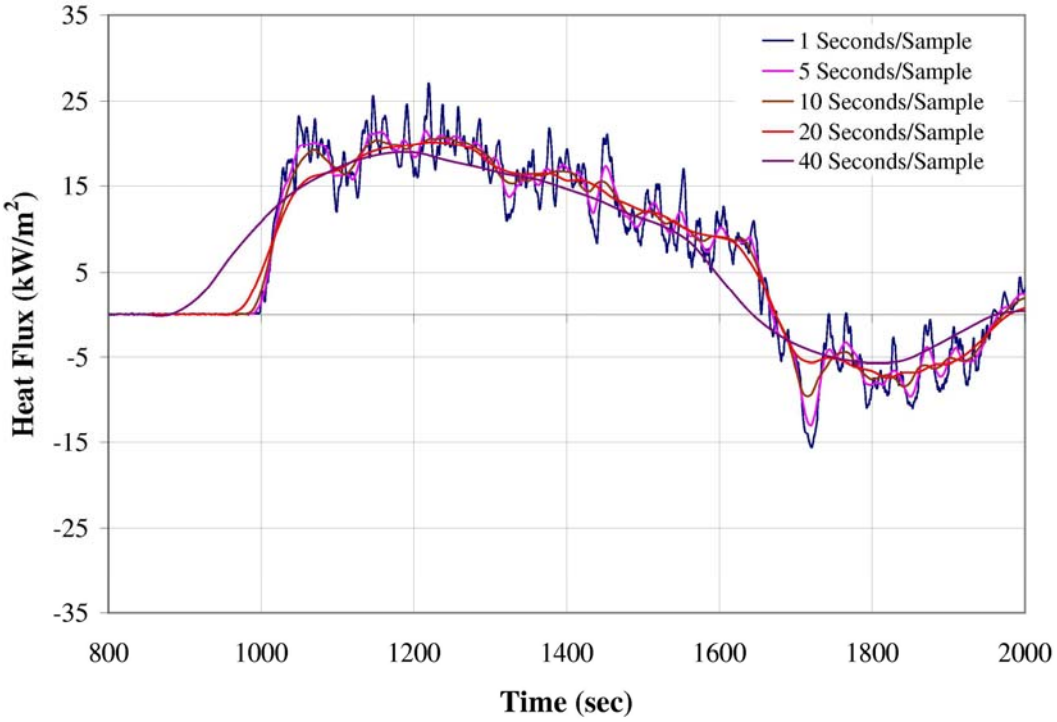

Figure 7: Calculated heat flux for various sampling periods.

5) Effects of Numerical Inputs on the Base-Case Results

Choice of numerical inputs will affect the estimation of heat flux. These inputs are often chosen based on recommended values in [1]. Three numeric inputs were studied: (1) number of nodes, (2) number of calculated time steps per measure time step, and (3) number of future times.

Figure 8 shows relative difference in the absorbed heat flux when the number of nodes-per-region was varied. These results were obtained by comparing the heat flux solution for 5, 10 and 30 nodes-per-region against the solution obtained with 50 nodes-per-region. Differences in maximum heat flux were progressively smaller with an increase in the number of nodes, suggesting grid convergence. Differences with the 50 node case were negligible when 30 nodes-per-region were used. Therefore, the number of nodes-per-region for the base-case was set to 30.

Heat flux differences between cases were negligible (data not shown) when the number of "calculated time steps-per-measure time step" was varied, so the default value of 10 was used.

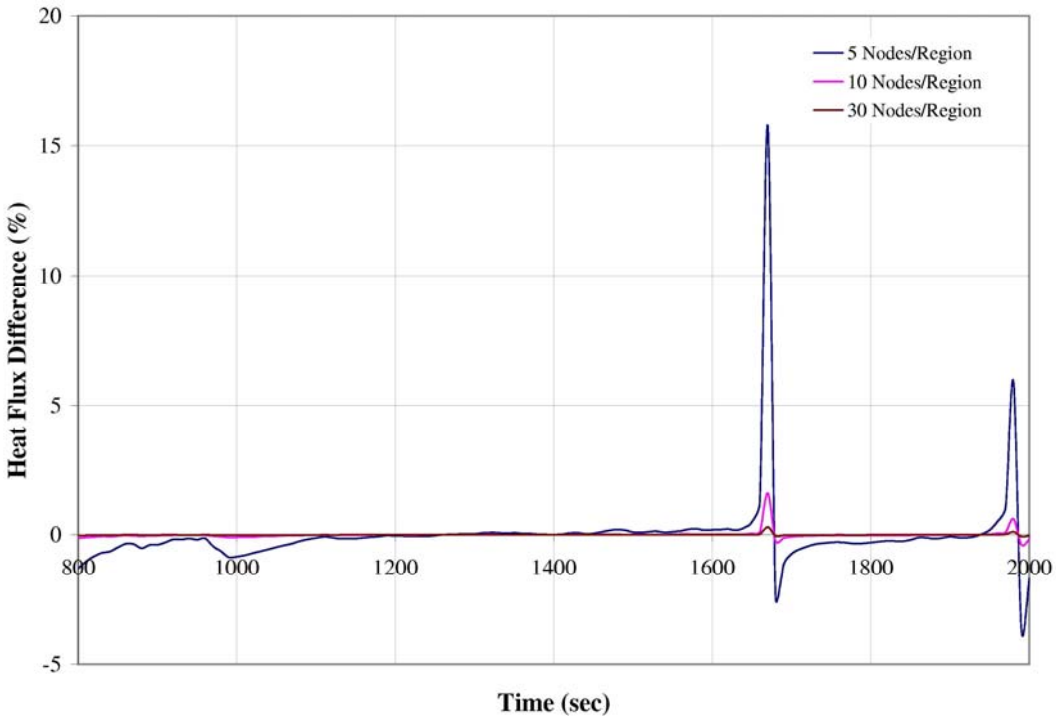

Figure 8: Differences in heat flux when the number of nodes was increased from 5 to 30 nodes-per-region.

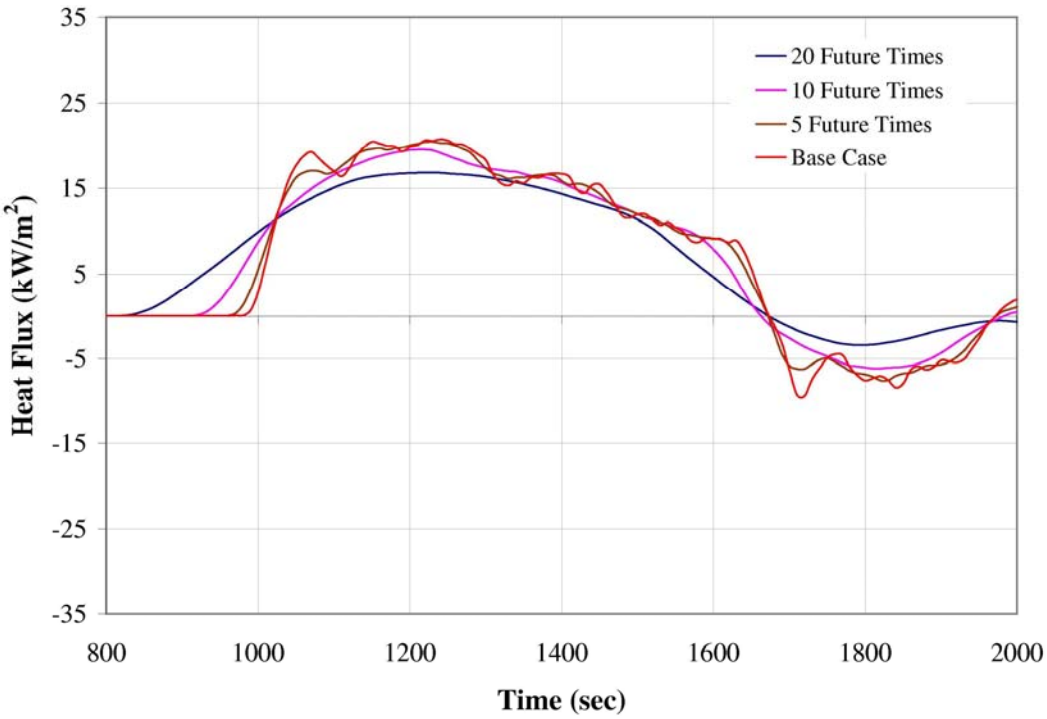

Figure 9: Damping and curve shift effects due to increases in the number of future time steps.

Figure 9 shows the impact of increasing the number of future times on the computed heat flux. Increasing the number of future times had a damping effect on the flux. Data using 10 and 20 future times shifts the results forward in time and severely damps the maximum flux values, so these future time values were not used. The smoothing and time shifting is not desirable. $r < 3$ is not desirable from a stability standpoint (see earlier discussion). Therefore, $r = 3$ was chosen as the best value because of minimal time shift and damping.

6) Effects of Using Constant Thermal Properties on the Base-Case Results

The use of constant thermal properties as opposed to variable properties significantly affects the calculated heat flux. Three cases were run so results could be compared with the base-case in which all properties varied with temperature:

- One case with constant thermal conductivity (14.52 W/m-°C),
- One case with constant volumetric heat capacity (3,734,430 J/m³-°C), and
- One case with both constant thermal conductivity and volumetric heat capacity (see Table 2).

Figure 10 shows the heat flux difference for the 3 cases. The largest differences were observed when the volumetric heat capacity and the thermal conductivity were both held constant, and when the volumetric heat capacity was constant. In both cases, peak differences were close to -14%. There was only a very small difference between results of constant volumetric heat capacity and thermal conductivity, and constant volumetric heat capacity. This suggests that the differences in both cases are entirely due to volumetric heat capacity.

In the case of insulation (Figure 11), the reverse behavior was observed. The largest difference as compared to the base-case was observed when the thermal conductivity was constant, and when the thermal conductivity and volumetric heat capacity were constant. For the insulation, the differences were almost entirely due to a constant thermal conductivity. Peak differences were about half (about 6%) of the values observed when the SS material properties were held constant.

These results showed the importance of using temperature-dependent properties for inverse heat flux calculations. Hence, temperature-dependent properties for both materials were used in subsequent runs.

B. Comparisons to Base-Case: Geometric, Thermal Property and Boundary-Condition Parameter Variations

A normalized heat flux difference at $x = L$ was used to compare results between cases. The normalized difference was calculated by taking the difference in absorbed heat flux and dividing the result by the maximum heat flux for the base-case:

$$\text{Normalized Heat Flux Difference}\,(\%) = 100 \cdot \frac{\text{Heat Flux(t)} - \text{Base Case Heat Flux(t)}}{\text{Base Case Maximum Heat Flux}}. \qquad (3)$$

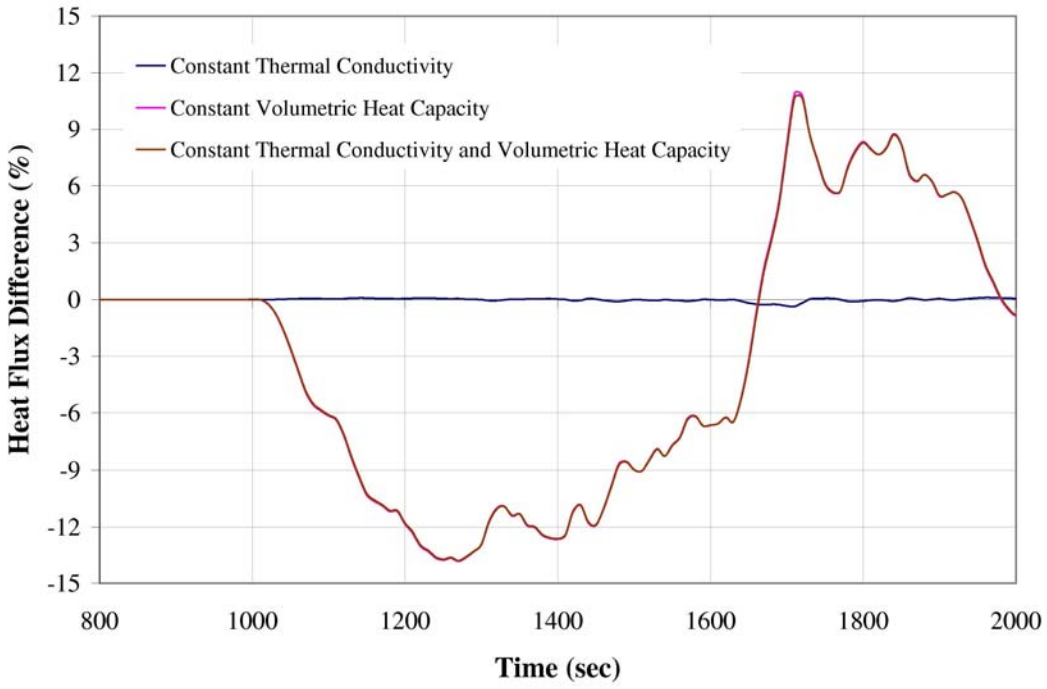

Figure 10: Normalized heat flux difference at $x = L$ using constant thermal properties for SS.

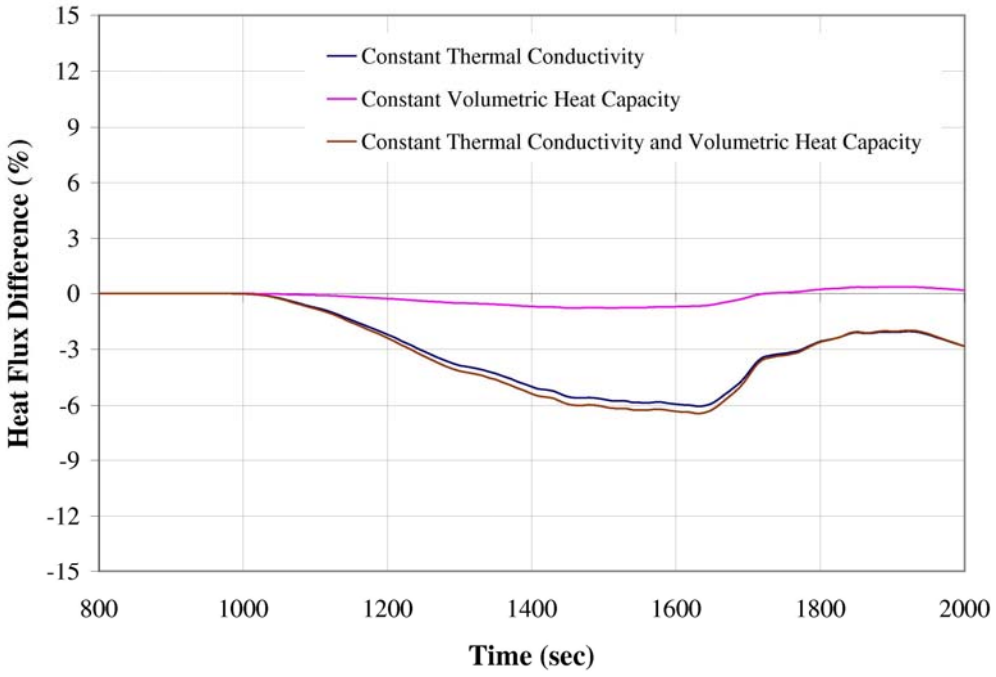

Figure 11: Normalized heat flux difference at $x = L$ using constant thermal properties for insulation.

This metric was chosen because small heat flux differences at low nominal heat flux levels can result in very large relative heat flux differences. At times when the nominal heat flux was low, large relative errors are not a concern; however, at times when the nominal heat flux was high, large relative errors are a concern. Therefore, the normalized heat flux difference is an appropriate metric for this study. Heat flux values were computed between 800 seconds and 2,000 seconds, when the heat flux was positive. Residual errors (between experimental and calculated temperature histories at the SS-insulation interface) were also checked for each case to ensure differences were acceptable (less than 1%).

1) Fixed Change (+5%) in Parameters

To determine the sensitivity on a consistent basis, the material thickness, thermal conductivity, volumetric heat capacity, and temperature history were varied by the same amount, 5%. Figure 12 shows the normalized heat flux difference for +5% changes in material thickness, thermal conductivity, heat capacity, and temperature. For the temperature history, 5% was added to each value of the original data set. In increasing order, the most significant heat flux differences were observed when the SS thickness (~4.5% at 1,150 seconds), volumetric heat capacity (~4.5% at 1,150 seconds), and temperature history (~5.6% at 1,240 seconds) were changed. For SS thickness and volumetric heat capacity, the change in heat flux was almost identical. This similarity was expected since the volumetric heat capacity and thickness of the cylinder both affected the volumetric term in the same manner. There were negligible heat flux differences—less than 0.5%—when the SS thermal conductivity and the insulation's thickness, thermal conductivity, and volumetric heat capacity were changed.

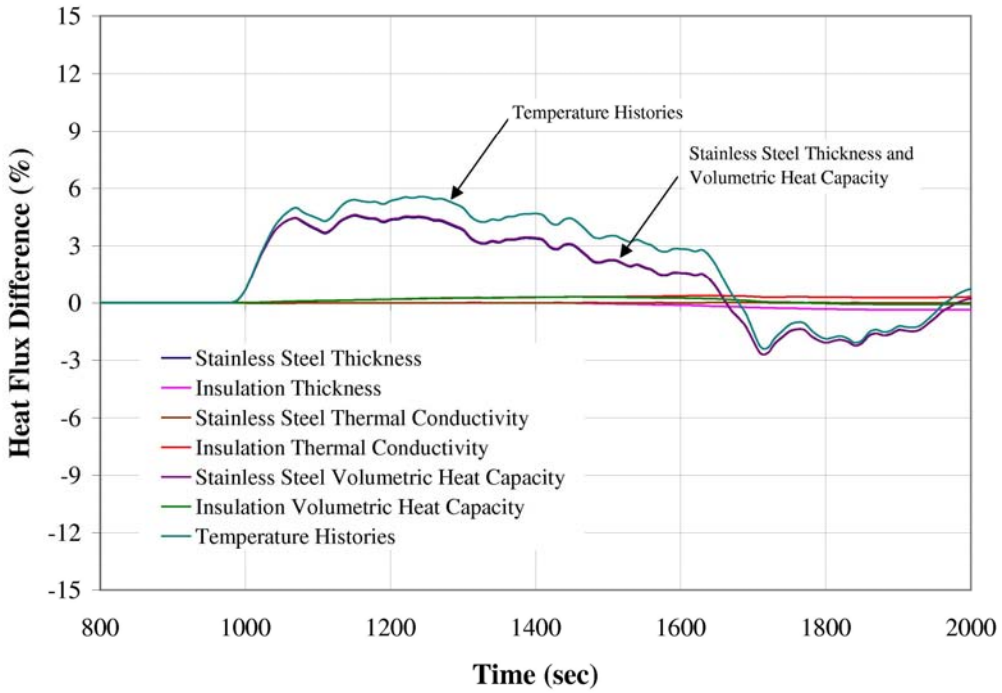

Figure 12: Percentage change in heat flux when temperature-dependent thermal properties, geometric dimensions, and temperature histories were changed by 5%.

The ratio of the relative change in heat flux to the relative change in the input parameter was used to determine sensitivity of the heat flux to the parameter variation [9, 10]. Thus,

$$UMF = \frac{X_i}{Y}\frac{\partial Y}{\partial X_i}. \tag{4}$$

This ratio is called the uncertainty magnification factor (UMF) or the normalized sensitivity coefficient [9]. X_i is the i^{th} input parameter, and Y is the output parameter (in this case, the heat flux). The partial derivative appearing in the equation is called the absolute sensitivity coefficient. When the UMF is greater than 1, the parameter variation's influence on the results amplifies; when the UMF is less than 1, the parameter variation's influence on the results diminishes.

Table 3 shows UMFs for the +5% variations in geometric, thermal property, and temperature-history variations. Heat flux differences at 1,240 seconds were used to calculate the maximum UMF. For the temperature history, the UMF was greater than 1; therefore, a 5% temperature error caused a larger error in heat flux (i.e., 5.6%). For all other parameters, the UMF was less than 1.

Table 3: Response of Heat Flux to Fixed Change (5%) in Geometric and Thermal Property Inputs

Parameter Changed	Uncertainty Magnification Factor (UMF)
Stainless-steel (SS) thickness	0.90
Insulation thickness	~ 0
SS thermal conductivity	~ 0
Insulation thermal conductivity	0.04
SS thermal capacity	0.91
Insulation thermal capacity	0.05
Temperature histories	1.12

2) Different Change in Each Parameter

Not all parameters have the same level of uncertainty (e.g., 5%). Total uncertainty in the inverse heat-conduction calculation was not only a function of the parameter sensitivity, but also a function of the magnitude of the uncertainty in each of the variable inputs [10].

Figures 13, 14 and 15 show the normalized heat flux difference when the geometric dimensions, thermal properties, and temperature history values were varied by the amount believed to be representative of the real application's uncertainty. Each parameter was varied by the same amount (both positive and negative). Table 4 shows a summary of the parameter changes. As in the previous section, the highest differences were observed when the temperature histories, SS thickness and SS volumetric heat capacity were changed. This time, however, the SS thickness (9% at 1,150 seconds) was the most significant parameter, followed by the SS volumetric heat capacity (4.5% at 1,150 seconds) and temperature history (2.8% at 1,220 seconds). Other parameters that contributed to the heat flux difference included the insulation-thermal conductivity (2.5% at 1,640 seconds) and volumetric heat capacity (1.5% at 1,460 seconds).

Table 4: Parameters Changed in Multi-Parameter Case

Parameters	Uncertainty Percentage	UMF
Steel thickness	10	0.90
Insulation thickness	10	~ 0
Steel thermal conductivity	2.5	~ 0
Insulation thermal conductivity	25.0	0.04
Steel volumetric heat capacity	5.0	0.91
Insulation volumetric heat capacity	25.0	0.05
Temperature measurement	2.5	1.12

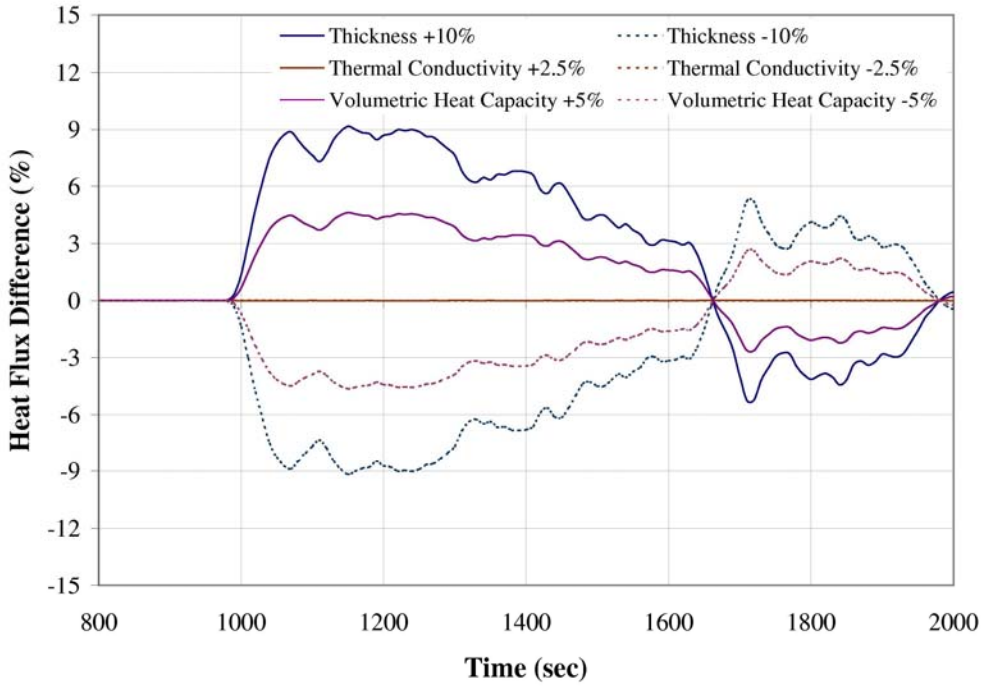

Figure 13: Normalized heat flux difference for changes in SS geometry and SS thermal properties.

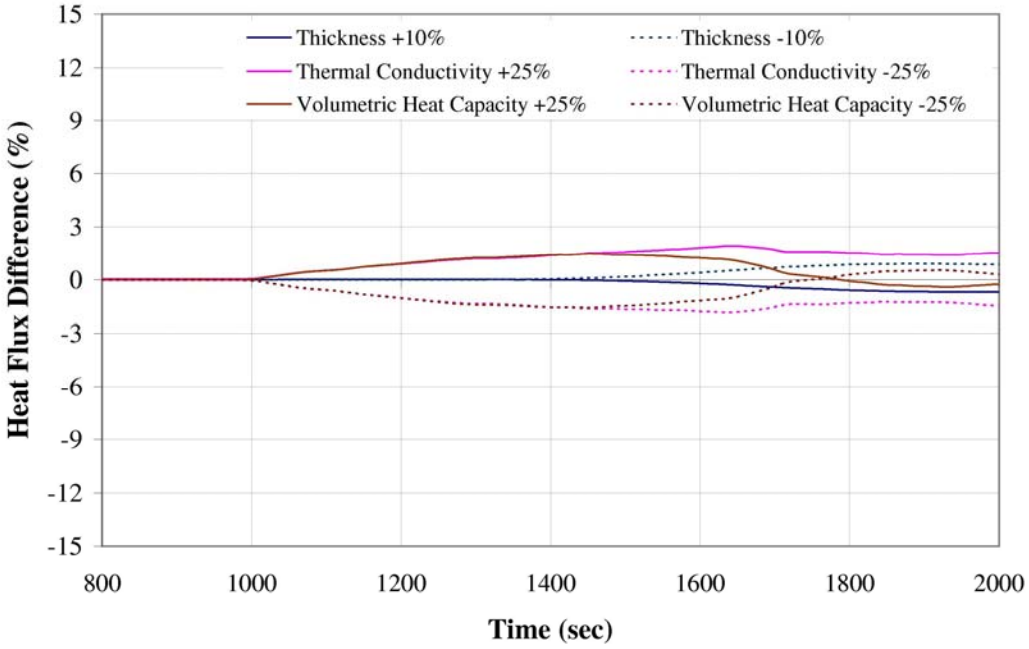

Figure 14: Normalized heat flux difference for changes in insulation geometry and insulation thermal properties.

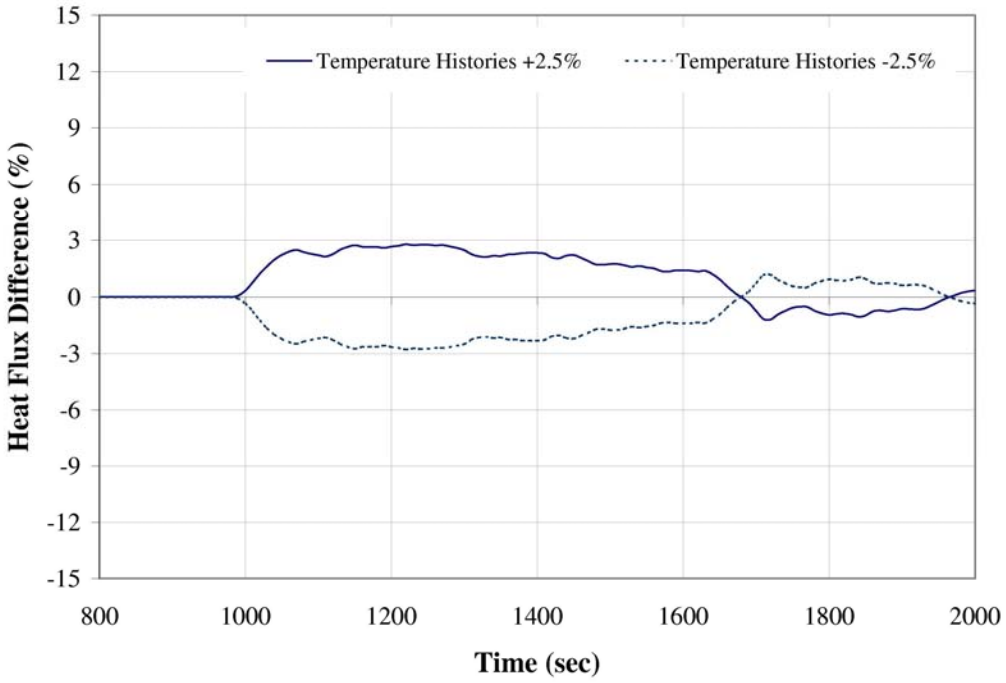

Figure 15: Normalized heat flux difference for changes in temperature history (only temperature on SS-insulation interface was varied)

As expected, the net effect on the heat flux was approximately linear with respect to the change in the input-parameter variations; hence, the symmetric effect is seen in Figures 13-15.

C. Total Uncertainty When All Parameters Were Changed Simultaneously

In each of the cases previously presented, only one parameter was changed for each run. In the following example, multiple parameters were changed to investigate interactions representative of the application. Numeric and sampling period parameters were not varied because these were not uncertainties found in the experiments, but rather bias effects introduced by the analyst when performing the inverse heat conduction calculation. Table 4 shows the parameters changed for this calculation. The UMF values were taken at the time of peak absorbed heat flux at $x = L$, which was 1,240 seconds. The total uncertainty was estimated using three different methods:

1. root-sum-square method.
2. the "additive" method.
3. uncertainty obtained from IHCP1D calculations.

For these calculations, it was assumed that the uncertainties were known to 95% confidence. This assumption includes some engineering judgment.

1) Uncertainty Analysis Using Root-Sum-Square and Additive Methods

The uncertainty analysis method outlined in [9] was used to estimate the total uncertainty in the calculated heat flux. The parameters, their corresponding uncertainty percentages, and UMF factors are given in Table 4. These parameter uncertainties were not separated into systematic and random uncertainties. The root-sum-square (RSS) method was used to estimate total uncertainty:

$$\frac{U_Y}{Y} = \sqrt{\sum \left(\frac{X_i}{Y} \frac{\partial Y}{\partial X_i} \right)^2 \left(\frac{U_{X_i}}{X_i} \right)^2} \quad , \tag{5}$$

where U_y is the absolute uncertainty in the heat flux, Y is the maximum heat flux, and U_{Xi} is the absolute uncertainty of each parameter. Other terms were defined in equation (4). The left and right terms inside the square root are the UMF and the relative uncertainty, respectively. This equation assumes that the measured variables X_i and the uncertainties U_{Xi} are independent of one another. The result of the RSS method is at a 95% confidence level (2σ) [11]. With the values in Table 4, the total uncertainty at 1,240 seconds was about 10.6% at a 95% confidence level.

If all the individual uncertainties from Figures 13-15 are added, the resulting value for total uncertainty is about 18.2%. Interpreting this larger value (18.2%) as an "additive" uncertainty, with a 99% confidence level (3σ) [11], one needs to modify it so a direct comparison can be made with the RSS value (10.6% at 95% confidence level). Adjusting the confidence level of the "additive" uncertainty from a 99% to a 95% gives 12.3%. This value is slightly higher than the 10.6% value obtained using the RSS value.

2) Uncertainty Analysis Using Results from IHCP1D

To compare with the RSS value, the input parameters in Table 4 were entered into IHCP1D, and the results were used to estimate the change in heat flux. The resultant uncertainty at 1,240 seconds was 14.3%. This value is interpreted at 95% confidence level because the input values used were at 95% confidence level [9]. The absolute uncertainty at 1,240 seconds was 2,958 W/m^2. Figure 16 shows the nominal error with upper and lower limits for the time period between 800 and 2,000 seconds, assuming negative uncertainties have the same value as the positive uncertainties.

The uncertainty value obtained from this calculation is higher that values obtained using the RSS and the "additive" methods. The difference (3.7% and 2.0% for RSS and additive methods, respectively) is believed to be due to non-linear effects not accounted for in the RSS or the "additive" method.

It is recommended that one use this method for estimating the total uncertainty, because it includes all linear and non-linear effects, and because it is cost effective to implement, only requiring two runs – the base-case and the run with all parameters varied at once.

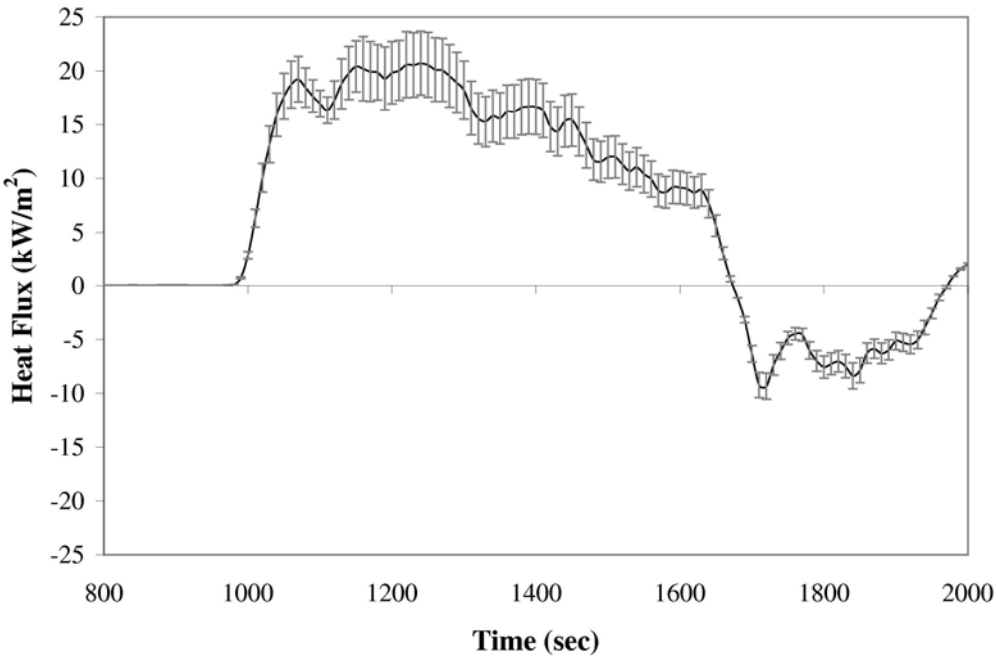

Figure 16: Error margin between the base-case and multiple-parameter case.

V. Discussion

This analysis has shown that the most important factors when using an inverse heat conduction technique such as IHCP1D to estimate absorbed flux in this application were:

1) number of future time steps,
2) sampling period,
3) use of temperature dependent properties,
4) temperature uncertainty,
5) steel thickness, and
6) steel volumetric heat capacity.

Which parameter is most important depends on how much that parameter can vary (i.e., a fixed % for all parameters or by amounts believed to be the most realistic). For a fixed 5% change in all parameters, the most important parameter was the temperature uncertainty, followed by the SS thickness, then SS volumetric heat capacity. For different parameter uncertainties believed representative of application shown in Table 4, the SS thickness uncertainty was the most important, followed by the SS volumetric heat capacity, and then the temperature uncertainty.

The calculated uncertainty using the RSS method (UMFs) was 10.6% at 95% confidence level, while the calculated uncertainty using IHCP1D program was about 14.3% at 95% confidence level. The larger IHCP1D value is believed to be due to non-linear effects not accounted for in the RSS method formulation (equation 5). When summing the individual uncertainties from

Figures 13-15, the result is 18.2% at 99% confidence level, which resulted in a value of 12.3% at 95% confidence level, in good agreement with the weighted RSS value.

These uncertainty estimates do not include uncertainty due to 2-D or 3-D localized heat flux gradients [4]. This effect will increase uncertainty of the inverse heat flux calculations above the level previously indicated. In addition, the effects of changing the sampling period or number of future time steps were not included in the uncertainty. These parameters have a similar effect in that they both damp fluctuations in the heat flux and time shift the heat flux. For large sampling periods or large number of future times, the net effect was a significant bias in the heat flux curves resulting from the time shift and damping. The effect of these program inputs (# future times and sample period) on the results should be studied for each problem before data are reduced. Because the run times IHCP1D are minimal (less than 5-10 seconds), it is cost effective to study these inputs before reducing all the data.

The transient response of the thermocouple can also affect the results. In our application, the frequency content of the input temperature was affected by limitations in the thermocouple transient response, and due to bias errors present when one attaches a thermocouple to a metal surface. No effort was made to correct the thermocouple temperature history before processing the data. The effect of these errors we believe to be quantified by assuming there is a temperature error of about 5%, as discussed earlier.

Long sample periods and a large number of future times caused a time shift at the beginning of the fire. For large sample periods (e.g., 20 and 40 seconds per sample), the beginning of the rise in flux time shifted forward (see Figure 7) which is not acceptable because the time shift could cause conflicts when comparing experimental data to model predictions. In addition, longer sampling periods or larger number of future times smoothed the peaks. It is difficult to judge whether or not the peaks are real or an artifact of the temperature data (see Figure 7). Engineering judgment is required.

Total uncertainties for each parameter should not be the only criteria for judging results; sensitivity coefficients also should be a determining factor. As Table 4 shows, a 5% change in temperature histories resulted in a slightly larger change—by a factor of 1.12 in maximum heat flux. In the case of volumetric heat flux and thickness, a 5% change in these parameters had a smaller effect (UMF = 0.91) in the results. Other factors (such as the insulation properties and thickness) had a negligible impact on the heat flux. Results shown in Table 4 are important because they demonstrate the importance of having an accurate assessment of the uncertainty for variables with relatively large sensitivity factors. In this study, the maximum sensitivity factor was 1.12; however, it is possible that with different test configurations, the maximum sensitivity factor could be larger.

If one adds the uncertainties from the example (10.6-14.3%) to the assumed 5% error in the base-case peak flux, the total uncertainty is from 15.6% to 19.3%. To be conservative an uncertainty of 20% can be assumed.

VI. Conclusions and Recommendations

A. Conclusions

Conclusions are as follows:

A) Differences in the sampling period and number of future times resulted in significant changes in heat flux (Figs. 7 and 9) due to smoothing and time shifting.

B) When the sampling period was too long or the number of future times to large, information may be lost due to smoothing peaks and time shifting the flux.

C) Results showed changes in heat flux using temperature-dependent properties were very significant (Figs. 9 and 11). Using temperature-dependent values for SS and insulation will result in more accurate estimation of heat flux.

D) During the fire, when the flux was positive, the heat flux change assuming an adiabatic-boundary condition on the SS-insulation interface or an adiabatic boundary condition at the center of the cylinder, as compared with the prescribed temperature boundary condition at the insulation-insulation interface, was negligible. But the difference was non-negligible after the heat flux went negative (after the fire was out) see Appendix C. Therefore, the thermocouple in the insulation was not required if one was interested only in the positive heat flux portion of the test. If resources or space is limited, the insulation-insulation TC can be eliminated. However, it can be used as a check and may be valuable in some cases, but care must be taken when mounting TCs in low conductivity materials because large errors can occur.

E) For a 5% change in all input parameters (see Figure 12), the most important factors were, in order of importance:

   1) Temperature uncertainty, SS thickness, and SS volumetric heat capacity.

   2) Parameter changes relating to insulation had a negligible effect on total uncertainty.

F) For representative uncertainties in input parameters (Table 4, and Figures 13-15), the most important factors were, in order of importance:

   1) SS thickness, SS volumetric heat capacity number, and temperature uncertainty.

   2) Parameter changes relating to insulation had a negligible effect on total uncertainty.

F) Total uncertainty for the case described in Table 4 was about ±10.6%, using a RSS (UMF) analysis. Using an additive method the total uncertainty was 18.2% for a 99% confidence interval (3). Adjusting this for 95% interval resulted in a 12.3%

uncertainty. If all parameters are varied at once, variations in heat flux using IHCP1D estimates a flux that is 14.3% different from the base-case, also assumed to be to 95% confidence. Non-linear effects accounted for the larger total uncertainty.

G) If one adds the uncertainties from the example (10.6-14.3%) to the assumed 5% error in the base-case peak flux, the total uncertainty is from 15.6% to 19.3%. To be conservative an uncertainty of 20% is recommended.

B. Recommendations

The authors make the following recommendations.

1) Carefully measure or otherwise obtain the density and specific heat of the steel being used. Use temperature dependent properties in the inverse calculations.

2) Carefully measure the steel thickness where temperature measurements are made.

3) Carefully quantify the temperature-measurement uncertainty, trying to reduce it as much as possible; consider both static and dynamic uncertainties. Use intrinsic or small diameter TCs to reduce the uncertainty.

4) Thermocouples on the back side of the insulation are not required if one is interested only in the positive heat fluxes. However, it is recommended that these measurements be made as a data check (i.e., to provide insight on 2-dimensional effects), but only if the measurement is made properly. Large TC errors (TC reads low) can result from placing a sheathed TC inside a low conductivity material like the Kaowool insulation. TCs should be mounted on a thin flat metal plate, then place the metal plate on the insulation.

5) Try several values for the number of future time steps; don't just use what has worked in the past, or use a default value. Three future time steps worked well for this application.

6) Try several sample periods to reduce data, and compare results before deciding on a final sample period to use. 10 seconds per sample worked well for this application, but shorter intervals may be more appropriate for a less thermally massive calorimeter in the fire to reproduce the higher frequency peaks.

7) Perform an analysis similar to the above to quantify total uncertainty for different calorimeters designs being used.

8) For this example (cylindrical calorimeter near but not in a fire), the absorbed heat flux uncertainty is estimated to be 20% using IHCP1D.

References

[1] J. V. Beck, "Users Manual for IHCP1D," a Program for Calculating Surface Heat Fluxes from Transient Temperatures Inside Solids, Beck Engineering Consultants Co., Okemos, Michigan, 48864, October 30, 1999.

[2] B. F. Blackwell, R.W. Douglass, and H. Wolf, "A Users Manual for the Sandia One-Dimensional Direct and Inverse Thermal (SODDIT) Code," Sandia National Laboratories report SAND85-2478, UC-32, Printed May 1987, Reprinted December 1980.

[3] M.N. Ozisik, "Heat Conduction," 2nd ed., John Wiley & Sons Inc., New York, 1993.

[4] C. Lopez, J.A. Koski, and A. Razani, "Estimate of Error Introduced When One-Dimensional Inverse Heat Transfer Techniques Are Applied to Multi-Dimensional Problems," in *Proceedings of Numerical Heat Transfer Conference*, (Pittsburgh, Pennsylvania, August 2000), NHTC2000-12037.

[5] J. J. Gregory, "Sensitivity Analysis for Noisy Temperature Data in Inverse Heat Conduction Calculations," Sandia National Laboratories memorandum, to N.R. Keltner, 1987.

[6] K.J. Dowding and B.F. Blackwell, "Sensitivity and Uncertainty Analysis for Thermal Problems," Sandia National Laboratories report SAND2001-1252P, 2001.

[7] K.J. Dowding, B.F. Blackwell, and R.J. Cochran, "Study of Heat Flux Gages Using Sensitivity Analysis," Sandia National Laboratories report SAND98-1758C, 1998.

[8] J.V. Beck, "Thermocouple Temperature Disturbances in Low Conductivity Materials", Journal of Heat Transfer, Trans. ASME 84C, May 1962, pp 124-132.

[9] H.W. Coleman, W. Glenn Steele, "Experimentation and Uncertainty Analysis for Engineers", 2nd ed., John Wiley & Sons Inc., New York, 1999.

[10] A. Saltelli, "What is Sensitivity Analysis?" in Sensitivity Analysis, A. Saltelli, K. Chan, and E.M. Scott, Eds. (John Wiley & Sons Inc., New York, 2000), pp. 10

[11] Measurement Uncertainty, Methods and Applications, Second Edition, by Ronald H. Dieck, ISA, 1997, pp 44-45.

Appendices

Appendix A: IHCP1D Screen Shots

The pictures presented in Appendix A are screen shots of the IHCP1D program used for this analysis. They are given in the step-by-step order in which information was input.

Appendix B: Input-Temperature Data

The file displayed in Appendix C gives the temperature values for interface one and the back face of the insulation, $x = 0$. Because of the large file sizes, only the values between 800–2,000 seconds were imported. These values corresponded to the heat flux values examined throughout this report.

Appendix C: Adiabatic-Boundary-Condition Case

For this analysis, it was assumed that the back face of the insulation, $x = 0$, was adiabatic. Other adiabatic-boundary conditions were considered. Results are shown in this section of the Appendix.

Appendix A: IHCP1D Screen Shots

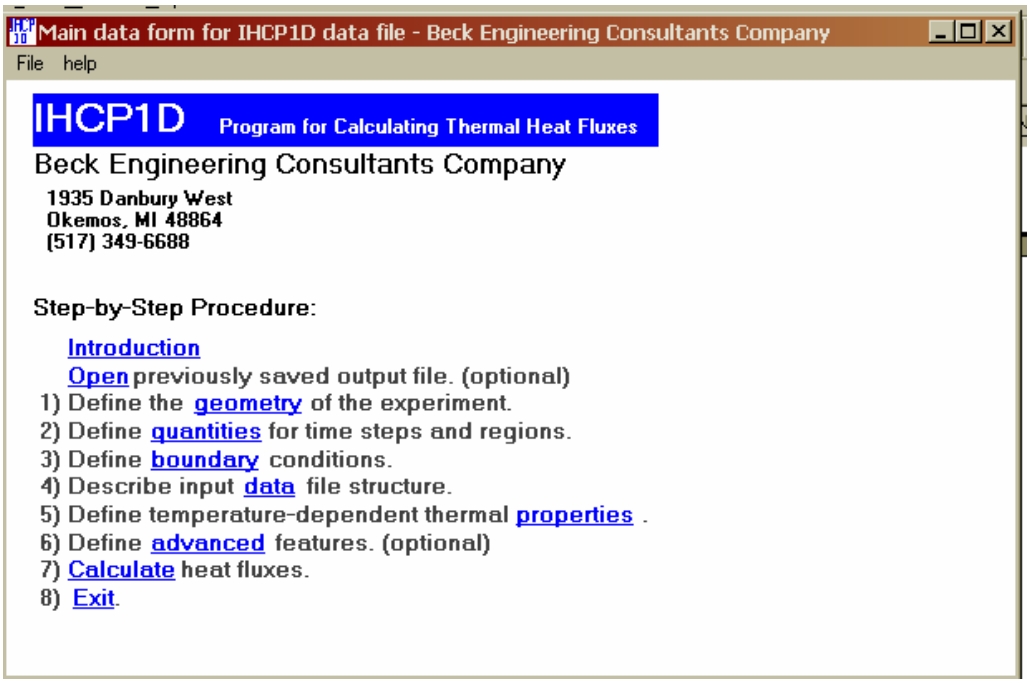

Figure A1: Initial screen.

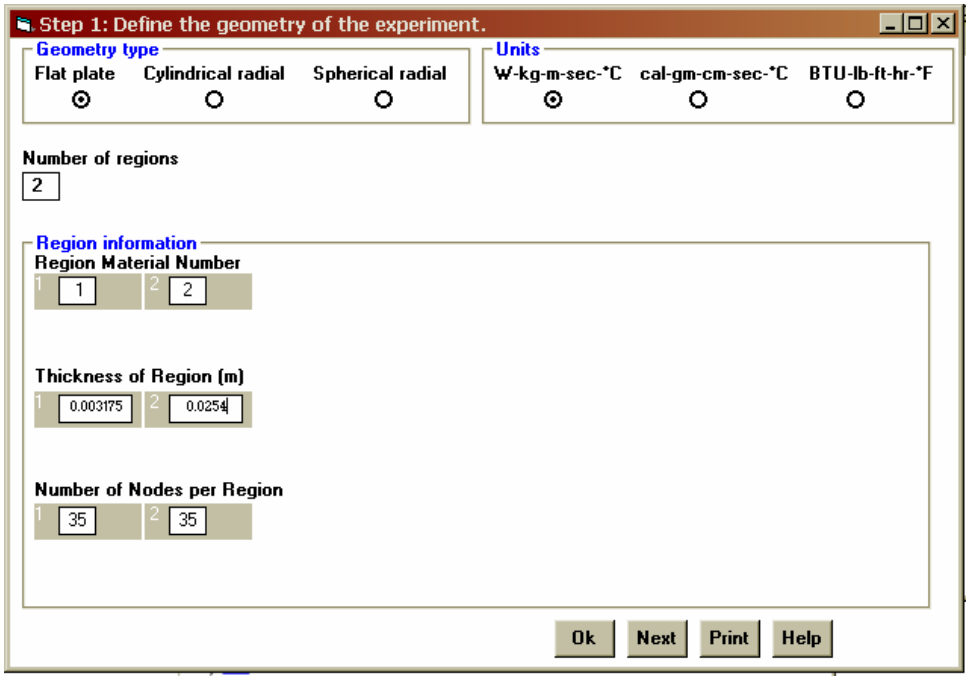

Figure A2: Step 1, define geometry.

Appendix A

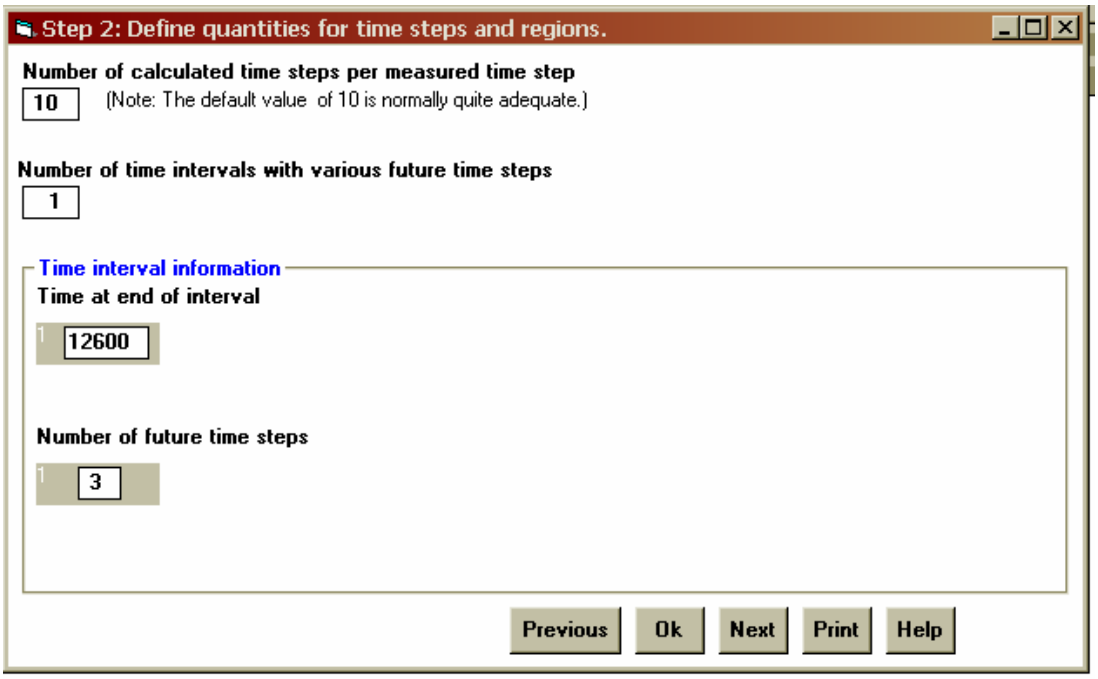

Figure A3: Step 2, define quantities for time steps and regions.

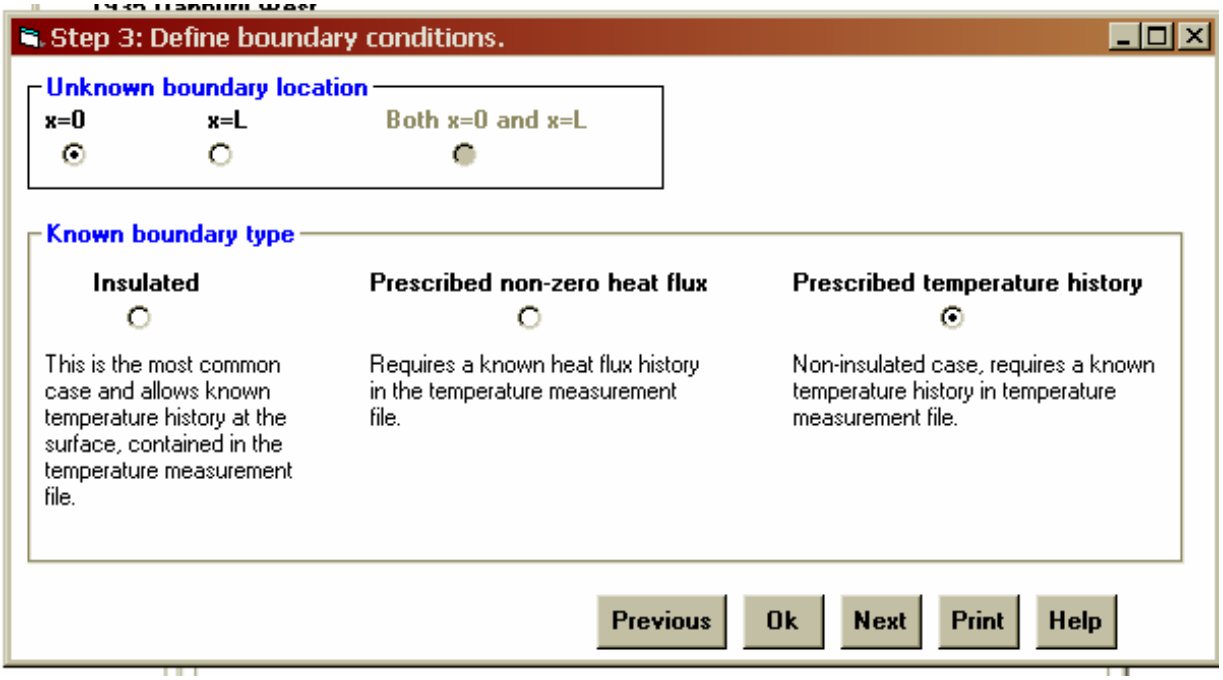

Figure A4: Step 3, define boundary conditions.

Appendix A

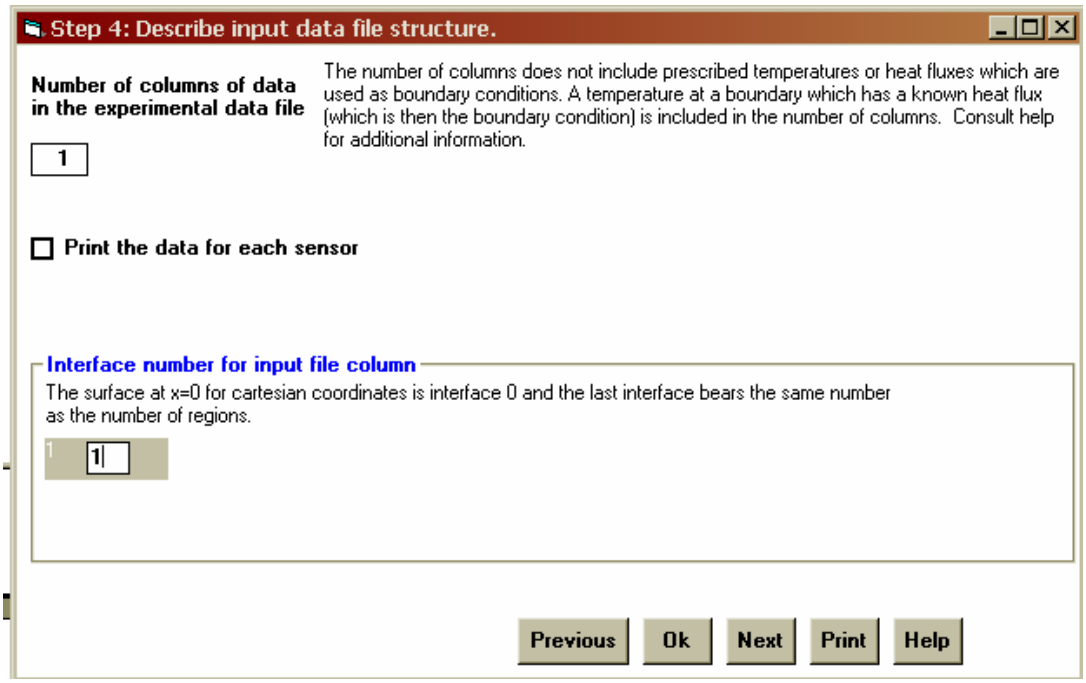

Figure A5: Step 4, describe input-data file structure.

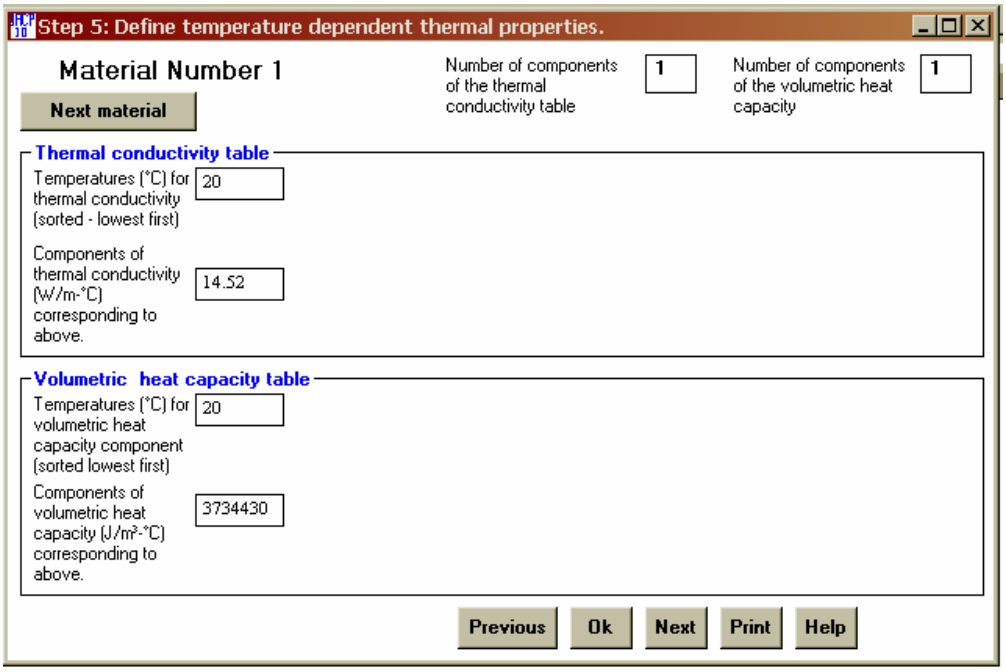

Figure A6: Step 5, define temperature-dependent thermal properties.

Appendix A

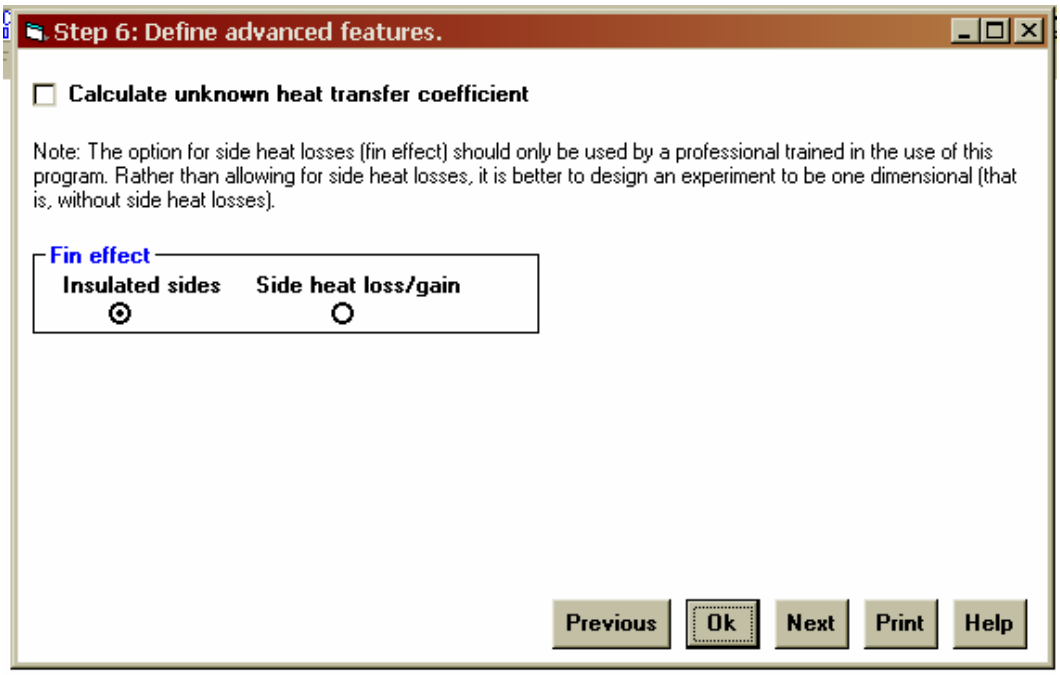

Figure A7: Step 6, define advanced features.

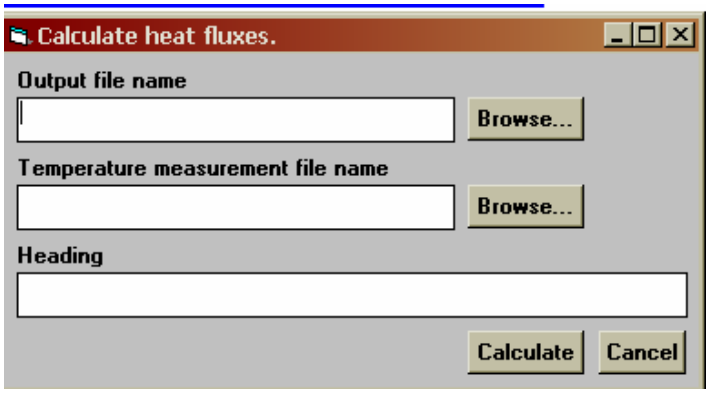

Figure A8: Step 7, calculate heat fluxes.

Appendix B

Appendix B: Input Temperature Data

Time	Interface Temp	BC Temp	Time	Interface Temp	BC Temp	Time	Interface Temp	BC Temp
800	19.32	20.24	1210	290.61	28.3	1620	645.16	276.48
810	19.32	20.27	1220	306.09	29.57	1630	649.58	284.99
820	19.34	20.28	1230	319.1	31.11	1640	653.27	293.44
830	19.35	20.31	1240	333.56	33.09	1650	658.34	301.91
840	19.37	20.31	1250	346.55	34.89	1660	658.55	310.28
850	19.38	20.29	1260	360.5	36.92	1670	657.65	318.44
860	19.41	20.34	1270	373.28	39.4	1680	654.74	326.31
870	19.41	20.37	1280	385.25	42.33	1690	650.88	333.53
880	19.42	20.34	1290	398.6	45.17	1700	647.22	340.38
890	19.44	20.37	1300	409.47	48.55	1710	640.79	346.59
900	19.48	20.38	1310	420.43	52.01	1720	630.17	352.38
910	19.48	20.39	1320	430.91	55.94	1730	620.1	357.19
920	19.51	20.35	1330	437.55	59.98	1740	615.76	361.83
930	19.52	20.38	1340	446.75	64.45	1750	613.68	366.3
940	19.53	20.34	1350	456.34	69.29	1760	608.77	370.08
950	19.55	20.3	1360	466.85	74.31	1770	606.48	373.72
960	19.56	20.34	1370	474.96	79.93	1780	602.56	377.14
970	19.58	20.35	1380	486.62	85.55	1790	597.89	380.52
980	19.59	20.33	1390	495.52	91.62	1800	590.14	383.05
990	19.65	20.28	1400	506.21	98	1810	584.24	385.61
1000	19.77	20.31	1410	516.09	104.34	1820	578.13	387.79
1010	22.16	20.25	1420	525.53	111.44	1830	573.48	389.91
1020	29.83	20.26	1430	534.49	118.65	1840	568.14	391.6
1030	41.9	20.21	1440	539.79	125.99	1850	561.09	393.37
1040	55.87	20.27	1450	548.89	133.38	1860	553.51	394.54
1050	70.55	20.25	1460	560.31	141.38	1870	549.95	395.64
1060	87.39	20.41	1470	567.49	149.36	1880	547.94	396.51
1070	102.58	20.47	1480	573.3	157.59	1890	542.02	397.09
1080	118.08	20.71	1490	579.1	165.91	1900	536.21	398
1090	132.86	20.8	1500	583.6	174.21	1910	533.41	398.19
1100	143.9	20.9	1510	590.7	182.37	1920	530.49	398.76
1110	156.12	20.98	1520	598.04	190.72	1930	524.85	399.16
1120	167.72	21.29	1530	603.69	199.27	1940	520.78	399.27
1130	178.4	21.89	1540	608.28	207.54	1950	518.09	399.3
1140	194.09	22.22	1550	613.33	216.18	1960	516.86	399.3
1150	209.94	22.75	1560	620.59	224.86	1970	516.21	399.32
1160	224.15	23.43	1570	623.66	233.55	1980	516.86	399.32
1170	239.2	24.07	1580	628.43	242.18	1990	516.87	399.32
1180	252.11	24.83	1590	631.15	250.81	2000	518.26	399.33
1190	265.44	25.89	1600	635.87	259.3			
1200	279.24	27.08	1610	641.75	267.94			

Appendix C: Adiabatic Boundary Conditions

Differences using a prescribed temperature-boundary condition and two assumed adiabatic-boundary conditions were analyzed. Results for prescribed temperature-boundary condition and two adiabatic-boundary condition cases were briefly described in the "Base-case" results section. A more detailed discussion is provided here.

Configuration 1: Center of the Cylindrical Calorimeter Is Adiabatic

For this case, it was assumed that the cylinder was uniformly heated, and the calorimeter's center was perfectly adiabatic. Figure C1 shows the model used in inverse heat flux calculations. The inner core material shown in light gray was the 0.1493-m-thick insulation.

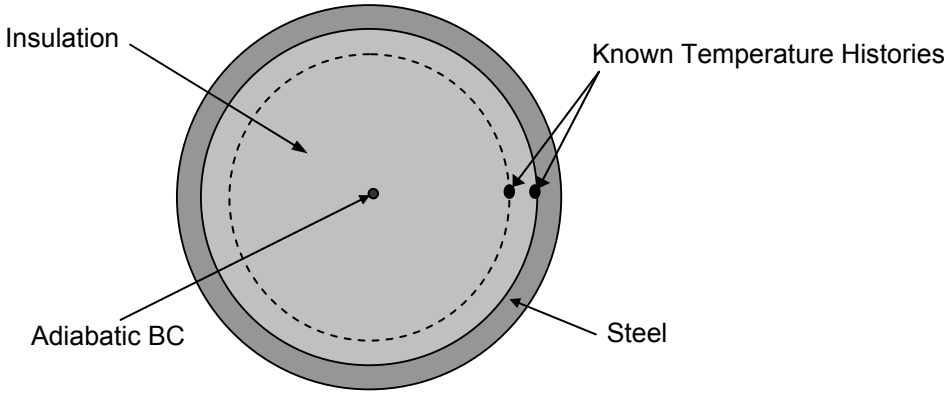

Figure C-1: Adiabatic-boundary-condition model.

The temperature history at the insulation-insulation interface was used in the base-case as the "prescribed boundary condition". In this case, an adiabatic boundary condition was prescribed at the cylinder's center. All numerical, geometric, and material property input parameters remained the same as in the base-case.

Figure C-2 illustrates the percentage difference if an adiabatic condition was chosen over a prescribed temperature-boundary condition. During the fire (200 to 800 seconds), the differences were minimal. As time progressed, however, differences were noticeable, up to about –3.7%. Because in the fire the cylinder was heated non-uniformly, there is no room to suspect the center was adiabatic. Therefore, this boundary condition was not used.

Appendix C

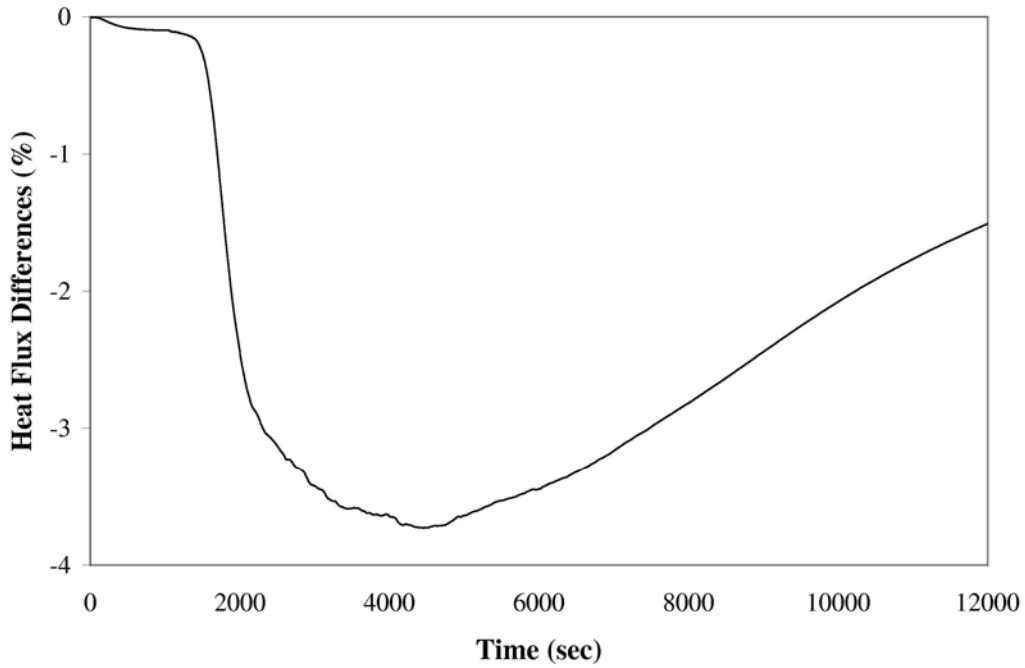

Figure C-2: Heat flux difference between use of adiabatic-boundary condition or prescribed temperature history in the calorimeter's center.

Configuration 2: Adiabatic Conditions behind 1-in. Insulation Layer

Figure C-3 shows results using adiabatic conditions at $x = 0$, the insulation-insulation interface. The heat flux difference is similar to Figure C2.

In both cases, an assumed adiabatic boundary condition, at either $x = 0$, or $R_i = 0$, resulted in a non-negligible error as compared with the results from the prescribed temperature history, but only after the absorbed heat flux went negative, after the fire was out. During the positive portion, when the fire was ongoing, the differences were negligible. Therefore, if the prescribed temperature history is known, it is recommended that it be used. However, because the estimated heat flux during the positive portion changes so little with the assumed boundary condition, an adiabatic boundary condition can also be used if the initial heat flux rise is the only portion of the calculation that is of interest. In this case the insulation-insulation thermocouple can be eliminated.

Appendix C

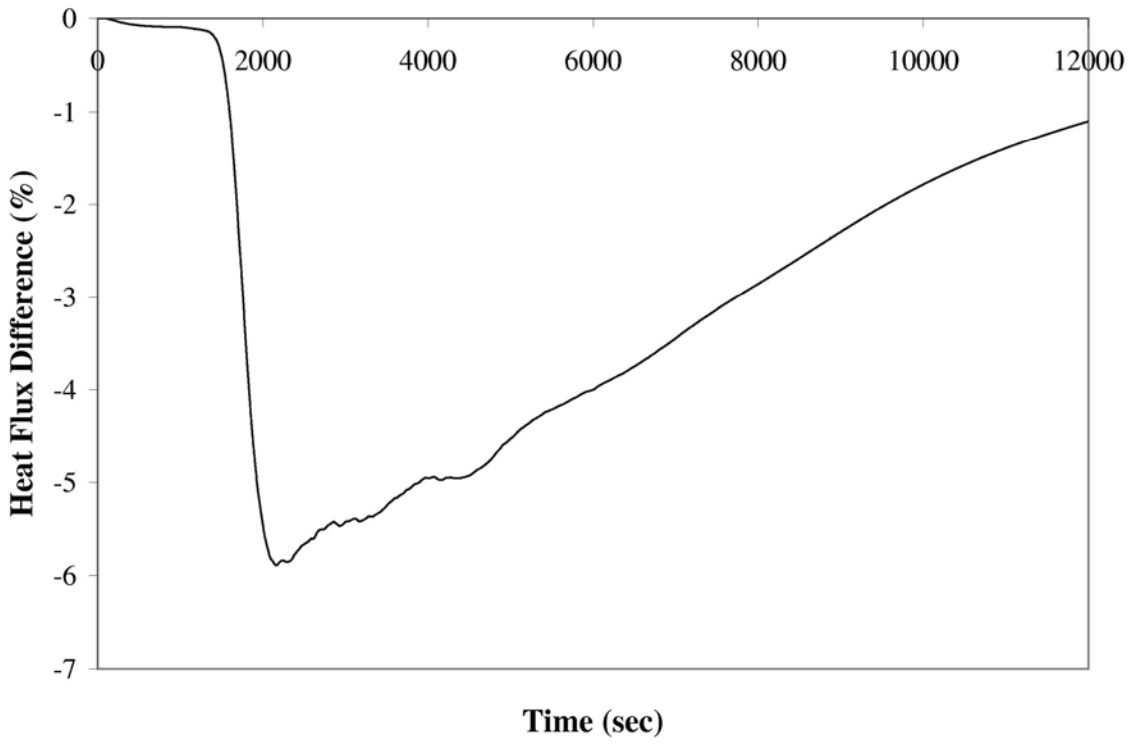

Figure C3: Heat flux difference using adiabatic-boundary conditions at $x = 0$.

Distribution

J.F. Nagel	MS0481, 2137
Tom Hendrickson	MS0481, 2137
Dennis Helmich	MS0481, 2132
Scott Slezak	MS0481, 2132
Alvin Leung	MS9014, 8242
Arthur Ortega	MS9014, 8242
Alfred Ver Berkmoes	MS9014, 8242
Carl Peterson	MS0384, 9100
T.Y. Chu	MS0834, 9110
Wahid Hermina	MS0834, 9120
Gene Hertel	MS0836, 9116
Lou Gritzo	MS1135, 9132
Martin Pilch	MS0828, 9133
Steve Heffelfinger	MS1135, 9134
Ken Erickson	MS0834, 9112
Sean Kearney	MS0834, 9112
Steve Trujillo	MS0834, 9112
Bruce Bainbridge	MS0836, 9116
Amanda Barra	MS0836, 9116
Barry Boughton	MS0836, 9116
Dean Dobranich	MS0836, 9116
Ron Dykhuizen	MS0836, 9116
Bill Erikson	MS0836, 9116
Nick Francis	MS0836, 9116
Roy Hogan	MS0836, 9116
Walt Gill	MS0836, 9132
Cecily Romero	MS0836, 9132
Tom Blanchat	MS1135, 9132
Jill Suo-Anttila	MS1135, 9132
Sheldon Tieszen	MS1135, 9132
Alex Brown	MS1135, 9132
Charles Hanks	MS1135, 9132
Dann Jernigan	MS1135, 9132
Sylvia Gomez	MS1135, 9132
Amalia Black	MS0828, 9133
Vicente Romero	MS0828, 9133
Martin Sherman	MS0828, 9133
James Nakos (3)	MS1135, 9132
Victor Figueroa (5)	MS1135. 9132
Jill Murphy, Worcester Polytechnic Institute (2)	
James Beck, Beck Engineering Consultants (1)	
Ned Keltner, Ktech Corp. (1)	
Ben Blackwell, Blackwell Engineering (1)	
Central Technical Files, 8945-1, MS9018	
Technical Library, 9616 (2), MS0899	